NUMERICAL ANALYSIS OF RADIATIVE TRANSFER OF A NON-GRAY FLAME USING STATISTICAL NARROW BAND METHOD

by

Melih Hilmi Bilgiç

B.S., Mechanical Engineering, Bogazici University, 2011

Submitted to the Institute for Graduate Studies in
Science and Engineering in partial fulfillment of
the requirements for the degree of
Master of Science

Graduate Program in Mechanical Engineering

Boğaziçi University

2014

This thesis is dedicated to my parents
for their love, endless support and encouragement.

ABSTRACT

NUMERICAL ANALYSIS OF RADIATIVE TRANSFER OF A NON-GRAY FLAME USING STATISTICAL NARROW BAND METHOD

Radiative heat transfer plays a significant role where high temperature participating gases exists, such as in boilers, jet engines and internal combustion engines. Analysis of such devices should include accurate radiative heat transfer calculations. In this work, radiative heat transfer in a flame is numerically analyzed using correlated-k statistical narrow band method. In order to achieve high order accuracy, current model utilizes k-distributions which are obtained from high temperature databases, namely HITEMP. Flame model is developed on a commercial software suit – Ansys FLUENT – on which all energy, fluid mechanics and chemistry equations are solved simultaneously. Radiative calculations are on another platform – MATLAB. Communications between these two software are established using TUI command of cfd software via MSDOS command. Radiative transfer equation is expressed numerically using discrete ordinates method in which 196 angular directions and 20x20 meshing are applied. In k-distributions, absorption coefficients - k values for each narrow band are presented with 7 point Gauss quadrature scheme. k-distributions are calculated for every species considered. CO_2 radiative properties are presented with 3 line parameters for 96 narrow bands of 25 cm^{-1} bandwidth, while 367 bands are used for H_2O of same bandwidth. Six verification cases are tested and compared with benchmark results to show that current model is at line-by-line accuracy. A turbulent hydrocarbon flame is modeled and non-gray solution is compared with gray solution. The results indicate that coupled cfd and accurate radiative heat transfer calculations using correlated-k narrowband model is feasible and gray model overestimates the emissions from the flame when compared to non-gray model.

ÖZET

GRİ OLMAYAN BİR ALEVİN IŞINIM YOLU İLE ISI TRANSFERİNİN İSTATİSTİKSEL DAR BANTLI METHOD İLE SAYISAL ANALİZİ

Buhar kazanları, jet motorları ve içten yanmalı motorlar gibi yüksek sıcaklıktaki gazların olduğu ortamlarda ışınım yolu ile ısı transferinin oynadığı rol çok önemlidir. Bu sistemlerin tasarim süreçlerinde ışınım yolu ile ısı transfer modellemesi zorunlu hale gelmektedir. Bu çalışmada bir alevin ışınım yolu ile ısı transferinin sayısal olarak modellenmesi ilintili-k istatistiksel dar bantlı model ile yapılmıştır. Yüksek doğrulukta (line-by-line) değeri ile eşdeğer hesap yapılabilmesi için bu modelde HITEMP yüksek sıcaklık veritabanından elde edilen k-dağılımları kullanılmıştır. Alev modellemesi ticari bir yazılım olan Ansys FLUENT üzerinden yapılmıştır. Bu yazılım ile enerji, akışkanlar mekaniği ve kimyasal denklemlerinin hepsi aynı anda çözülmesi sağlanmıştır. Işınım transferi hesapları MATLAB üzerinden yapılmıştır. Bu iki platform arasındaki iletişim had (hesaplamali akışkanlar dinamiği) yazılımının TUI komutları ile MSDOS komutları üzerinden sağlanmıştır. Işınım transferi denklemi, ayrık ordinatlar yöntemi ile sayısal olarak ifade edilmiş olup denklem açısal olarak 196, uzaysal olarak da 20x20 bölgeye ayrılmıştır. Absorpsiyon katsayıları - k değerleri her bir dar bant için 7 noktalı Gauss tümlev şeması kullanılarak ifade edilmişlerdir. CO_2 ışınım özellikleri 3 çizgi parametresi ile 96 dar bant için 25 cm^{-1} bant genişliği kullanılarak, H_2O ise aynı şekilde ama 367 dar bant ile ifade edilmiştir. 6 doğrulama vakası ile benchmark değer karşılaştırması yapılıp, mevcut modelin line-by-line doğruluğunda olduğu görülmüştür. Türbulanslı hidrokarbon alev modellemesi yapılıp gri olmayan vaka, gri vaka ile karşılaştırılmıştır. Sonuçlar had ve ilintili-k istatistiksel dar bantlı model kullanan ışınım hesaplamalarının yüksek doğrulukta (line-by-line) yapılabilecegi ve gri ortam kabulu ile yapılan hesaplamalarla alevden ışımanın gri olmayan ortama göre daha yüksek olduğunu göstermiştir.

TABLE OF CONTENTS

LIST OF FIGURES

LIST OF TABLES

LIST OF SYMBOLS

a_j	WSGG weights
B	SNB model parameter
c_p	Specific heat at constant pressure
E	Total energy
f	Distribution function
g	Cumulative distribution function
h	Sensible enthalpy
H	Heavisides unit step function
$\hat{\imath}$	X-component of unit directions in Cartesian coordinates
I	Radiative intensity
I_η	Spectral radiative intensity
I_b	Blackbody radiative intensity
$\hat{\jmath}$	Y-component of unit directions in Cartesian coordinates
j	Index
J	Number of gray gases in WSGG
k	Absorption coefficient or thermal conductivity
$\hat{k}$	Z-component of unit directions in Cartesian coordinates
$\bar{k}_v$	Mean line-intensity to spacing ratio
L	Gas column path-length (m)
M_w	Molecular weight
n	Refractive index
$\vec{n}$	Normal direction
p	Pressure
p_s	Reference pressure
q	Heat flux
$\vec{r}$	Position vector
s_w	Position vector along wall
$\vec{s}$	Direction vector of rays
S	SNB model parameter

S_h	Heat source in energy equation
t	Time
T	Temperature
T_s	Reference temperature
u_i	Velocity component
$\bar{u}_i$	Mean velocity
u_i'	Fluctuating velocity component
W_i	Weight parameter of the ith Gauss quadrature point
W_x	X component of positive scheme weights
W_y	Y component of positive scheme weights
x_i	Cartesian coordinates
x	X component of Cartesian coordinates
X	Molar fraction
y	Y component of Cartesian coordinates
Y_i	Mass fraction of species i
$\bar{\beta}_v$	Mean line-width to spacing ratio
$\bar{\gamma}_v$	Mean half-width of an absorption line
$\bar{\gamma}$	Ratio of specific heats
$\Delta\eta$	wave number interval
δ	Dirac's delta function or unit tensor
ϵ	Emissivity
ε	Turbulence model parameter
η	wave number or x component of direction cosine
θ	Polar angle
κ	Absorption coefficient
κ_η	Spectral absorption coefficient
κ_j	Gray gas absorption coefficient in WSGG
$\kappa_{p\eta}$	Pressure-based spectral absorption coefficient
λ	Wavelength
μ	Viscosity

ν	Frequency
ν', ν''	Stoichiometric coefficient for reactants and products
ξ	Y component of direction cosine
ρ	Reflectivity or density
σ	Stefan-Boltzmann constant
$\sigma_{\eta s}$	Spectral scattering coefficient
$\bar{\tau}_{\eta}$	Averaged spectral transmissivity
Φ	Scattering phase function
Ψ	Azimuthal angle
ω_i	I^{th} quadrature of discrete ordinates
Ω	Solid angle

LIST OF ACRONYMS/ABBREVIATIONS

EM2C	Le laboratoire d'Énergétique Moléculaire et Macroscopique, Combustion
HITEMP	High-temperature molecular spectroscopic database
HITRAN	High-resolution transmission molecular absorption database
LBL	Line-by-line
RTE	Radiative transfer equation
WSGG	Weighted-sum-of-gray-gases
SNB	Statistical narrow band
SNBCK	Statistical narrow band correlated-k

1. INTRODUCTION

Radiative heat transfer plays a significant role in many scientific and engineering fields, such as aeronautics, astronautics and mechanics and it is also dominant mode of heat transfer in many engineering devices such as furnaces and boilers where there is an enclosure filled with combusting gas mixture at high temperature. Therefore in thermal modeling of flames, accurate estimation of radiative heat transfer is essential in order to predict the temperature distribution within the flame.

A combustion environment generally consists of multidimensional enclosures containing participating gases which absorb and emit electromagnetic waves. In the absence of soot the scattering of the electromagnetic waves is mostly negligible for combustion gases. The radiative properties of the medium consisting mixture of gases have spatial, angular and spectral dependencies. Absorption coefficient will be the most important one among these properties. In addition, the medium is generally non-homogeneous which means inhomogeneity occurs within medium in terms of pressure, temperature and molar composition gradients across gas layer. The methods are proposed to obtain exact and approximate solutions of radiative transfer equation (RTE) can be loosely grouped into four, namely line-by-line (LBL), narrow band, wide band and global models [1].

The most accurate model among these methods is LBL, which solves the RTE for each emission line. The radiative property data are obtained from spectrometric databases which contains millions of line data for molecular gases such as carbon dioxide and water vapor. Among the databases available; most common ones are the high-temperature molecular spectroscopic database and high-resolution transmission molecular absorption database under the acronyms of HITEMP [2] and HITRAN [3] respectively. The results of LBL calculations are the most accurate ones; however since they encompass millions of lines of data especially at elevated temperature, solution of RTE for all lines requires excessive cpu times and LBL calculations are not practical for engineering applications. Thus, LBL calculation is used as a benchmark result for

specific cases [4].

Narrow band model is a widely used model for engineering applications. Blackbody intensities within the narrow band of interest is constant. If, on the other hand, the absorption coefficient is observed across the spectrum, one can find that it varies much more than blackbody intensity. Thus, it is possible to reorder actual absorption coefficient and also intensity in a narrow band by smoothened ones in order to integrate spectral quantities in a more accurate and easier way. In principle, narrow band solutions can be as accurate as LBL. The main disadvantage of narrow band model is that its application to non-homogeneous gases is difficult; however, the solutions to non-scattering medium and black-walled enclosures is possible. More recently, correlated k-distributions are developed, in which rapidly oscillating absorption coefficient values are reordered according to how many times the same value of absorption coefficient in presented at different spectral positions. The resulting reordered function is called distribution function, which makes integration of spectral quantities more straightforward. This approach is relatively new and still difficult to apply for non-homogeneous media.

In wide band models, a larger wave number interval is used in the calculations in comparison to narrow band models. Although the blackbody intensity changes in a wide band, the variation in blackbody emission is not very substantial, even across an entire vibration-rotation band. Narrow band results are integrated across an entire band in wide band models, which give less accurate results. It was popular in the past due to its simplicity and that it requires less spectral data. Correlated k-distributions can be readily employed in wide band models as well, which is one of the attractions.

A global model is based on evaluating radiative properties for the entire spectrum. The main interest is to find total radiative heat flux or its divergence by using spectrally integrated radiative properties. The first examples use total emissivity and absorptivity of gas columns; however, full spectrum correlated-k distributions are also developed later [5].

The problem aim of this study is stated as to numerically find LBL accurate radiative intensity field of a two-dimensional hydrocarbon flame enclosed within black walls. Using radiative intensity field, spectral divergence of heat flux and wall heat flux are calculated. Second aim of the study is to couple radiative solver with a computational fluid dynamics (cfd) solver. A commercial cfd package is selected (Ansys FLUENT), which uses control volume techniques to discretize and solve governing equations of continuum, momentum, energy and species transport [7]. The main motivation to this study is that cfd solvers do not include LBL accurate radiative calculations. Integration of the radiative solution to a cfd program will lead to better control of spectral calculations and to obtain LBL accurate solutions to complex combustion problems.

To solve RTE is a challenging task, because of its inherited relation with electromagnetic waves and quantum mechanics. For that manner, many solution methods exist in the literature, while this study is only focused on discrete ordinates method. Both RTE and its solution method are discussed in detail in the next chapter. Spectral dependency of participating gases on absorption coefficient is taken into consideration using statistical narrow band correlated-k model which is also covered in Section 2.4. Using these models, RTE is solved in a non-gray participating medium consisting of water vapor and carbon dioxide. The calculations are done on MATLAB [8], a technical programming software, which are then verified according to Goutiere's work [9]. The details of RTE calculations are given in Section 2.6.

2. RADIATIVE HEAT TRANSFER

2.1. Radiative Transfer Equation

Radiative intensity I can be defined as the total radiative energy flow per unit solid angle Ω, per unit time t, per unit area normal to the rays. The spectral radiative intensity I_η is the intensity within an infinitesimal wavelength $d\eta$. The spectral notation of subscript η can be sometimes used substitutively with wave number η or frequency ν. The relation between spectral and total radiative intensity at a spatial location $\vec{r}$, and traveling in the direction $\vec{s}$ is given in Equation 2.1.

$$I(\vec{r},\vec{s}) = \int_0^\infty I_\eta(\vec{r},\vec{s},\eta)d\eta \tag{2.1}$$

A surface dA radiates rays in every possible direction which are crossing a unit hemisphere having a total area of 2π. The direction $\vec{s}$ is generally defined with polar and azimuthal angles namely θ and Ψ. An infinitesimal solid angle $d\Omega(\theta,\Psi)$ can be defined as the area on unit hemisphere whose corners are at the polar positions of $(\theta,\Psi+d\Psi)$, $(\theta+d\theta,\Psi+d\Psi)$, (θ,Ψ) and $(\theta+d\theta,\Psi+d\Psi)$. The infinitesimal solid angle is then given as $d\Omega(\theta,\Psi) = \sin\theta d\theta d\Psi$ and total solid angle is calculated by integrating in those two directions given in Equation 2.2. An infinitesimal solid angle in the direction of $\vec{s}$ is illustrated in Figure 2.1.

$$2\pi = \int_0^{2\pi}\int_0^{\pi/2} \sin\theta d\theta d\Psi \tag{2.2}$$

Electromagnetic waves travel at the speed of light so that the processes in the radiative heat transfer can be assumed to occur at infinitely fast rate. This assumption known as quasi-steady and time dependency of radiative heat transfer is neglected for many applications. The governing equation for the radiative heat transfer is the radiative transfer equation (RTE) in a particular propagation direction s and for quasi-steady

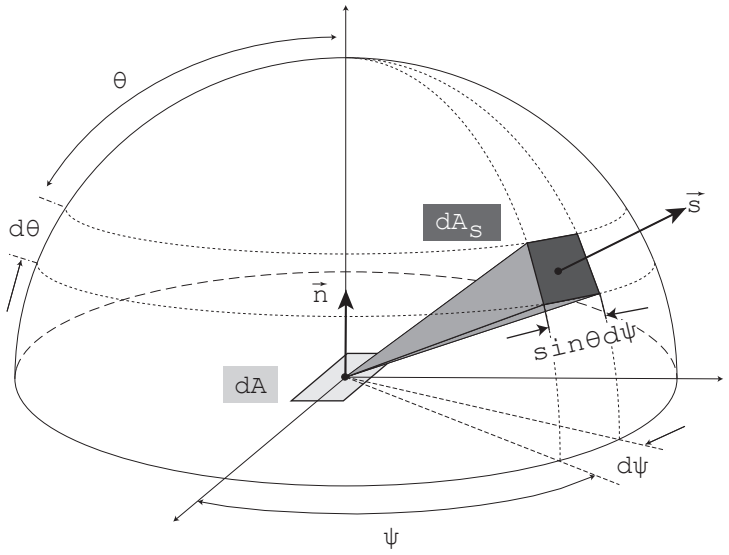

Figure 2.1: A solid angle as related with unit hemisphere.

conditions can be given in differential form as [10],

$$\frac{dI_\eta}{ds} = -(\kappa_\eta + \sigma_{\eta s})I_\eta + \kappa_\eta I_{b\eta} + \frac{\sigma_{\eta s}}{4\pi}\int_0^{4\pi} \Phi(\vec{s}\,' \to \vec{s}; \eta' \to \eta) I'_\eta(\vec{s}\,')d\Omega' \tag{2.3}$$

where $I_{b\eta}$ is the spectral blackbody radiative intensity, κ_η is the spectral absorption coefficient, $\sigma_{\eta s}$ is the spectral scattering coefficient, $\Phi(\vec{s}\,' \to \vec{s}; \eta' \to \eta) I'_\eta(\vec{s}\,')d\Omega'$, is the amount of energy flux from direction $\vec{s}$ that is scattered into direction $\vec{s}\,'$. The amount of change in spectral intensity due to the change in position in Equation 2.3 can be grouped into three terms.

- The first term of RTE is attenuation due to absorption and out-scattering
- The second term of RTE is augmentation due to emission
- The third term of RTE is energy gain due to in-scattering.

The radiative transfer equation is subject to boundary conditions, and a boundary condition for an enclosure with diffusively emitting and reflecting opaque walls

$$I(\vec{r}_w, \vec{s}) = \epsilon_\eta(\vec{s}_w) I_{b\eta}(\vec{s}_w) + \frac{\rho_\eta(\vec{s}_w)}{\pi} \int_{\vec{n}\cdot\vec{s}\,'<0} I(\vec{s}_w, \vec{s}\,')|\vec{n}\cdot\vec{s}|d\Omega' \tag{2.4}$$

where ϵ_η is spectral emissivity, ρ_η is spectral reflectivity, $\vec{n}$ is the direction normal to the surface, subscript w in $\vec{r_w}$ stands for wall position. Boundary condition shown in Equation 2.4 is limited to an enclosure with diffusely emitting and reflecting opaque walls; however other boundary conditions can also be applied such as specularly reflecting walls or arbitrary surface properties including semi transparent surfaces.

Radiative transfer equation is an integro-differential equation depending on wavelength, three spatial coordinates, two directional variables. Since analytical solutions are limited to very simple cases, many numerical solution methods are developed and given in the literature with their pros and cons [5, 10–12].

Before starting to model the radiative heat transfer in a combustion environment, key points may be given as follows [12]. The choice of radiative heat transfer model is the first step. Since, exact solution to radiative transfer equation is not available for engineering applications, some approximations such as omission of scattering should be made. Second step is to choose an appropriate model giving intensity-wavelength relation, since thermal radiative transfer shows higher order spectral dependence. A suitable band model or gray assumption should be taken into consideration and spectral part of the radiative transfer should be analyzed by using one of the numerical methods that is compatible with solution of the radiative transfer equation. The solution method should be accurate, robust and efficient and the model should work in a computationally efficient way and computed quantities related with radiant energy should be accurate.

In this study, radiative heat transfer equation is solved for a two dimensional, non-scattering, non-gray medium that is enclosed by black walls. The RTE with these assumptions depend on two spatial coordinates, a direction vector and wavelength. Solution is obtained using discrete ordinates method which relates spatial and directional

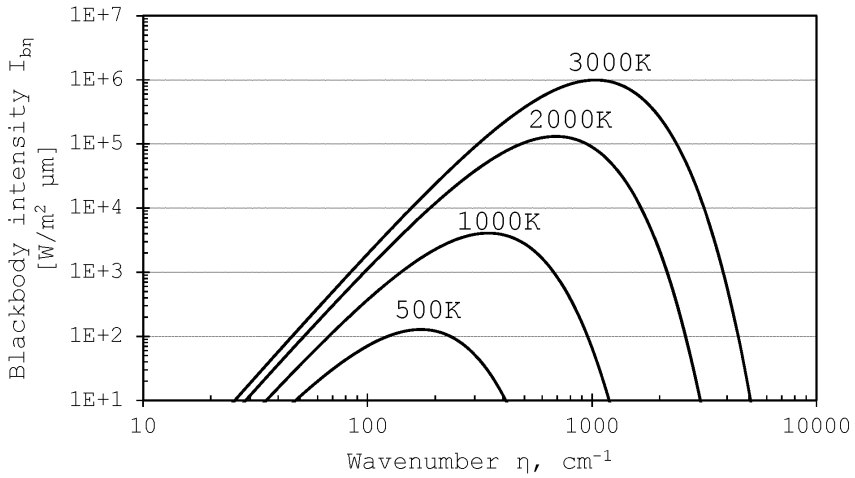

Figure 2.2: Blackbody intensity at temperatures of 500, 1000, 2000 and 3000 K.

dependencies with a good accuracy. An effort is made to model wavelength dependent radiative properties. Many spectral models are investigated, some of them are explained in detail such as k-distributions and weighted sum of gray gases. In addition, surfaces are treated as black in this study, which means all incoming intensity to the surface are absorbed; while black surfaces radiate according to Planck function which only depends on temperature and wavelength. The plot is given in Figure 2.2 showing change of blackbody emission intensity with wave number at body temperatures of 500, 1000, 2000 and 3000 K.

2.2. Radiative Intensity Solution Along a Path

If non-scattering medium and black boundaries are assumed, Equation 2.3 will be simplified to

$$\frac{dI_\eta}{ds} = \kappa_\eta (I_{b\eta} - I_\eta) \tag{2.5}$$

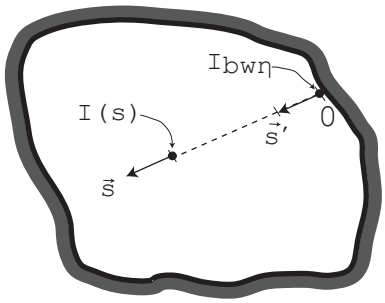

Figure 2.3: Spectral intensity within an arbitrary black-walled enclosure.

Formal solution to Equation 2.5 for the entire spectrum will be given in terms of radiative intensity $I(s)$ in the direction of $\vec{s}$ as

$$I(s) = \int_0^\infty I_\eta d\eta = \int_0^\infty I_{bw\eta} \exp\Big(- \int_0^s \kappa_\eta ds' \Big) d\eta + \int_0^s \int_0^\infty I_{b\eta}(s') \exp\Big(- \int_{s'}^s \kappa_\eta ds'' \Big) \kappa_\eta(s') d\eta ds' \quad (2.6)$$

where $I_{bw\eta}$ is the outgoing spectral intensity from black wall. An example to an intensity and its direction are illustrated in Figure 2.3. The spectral emissivity of a participating medium is defined in Equation 2.7 which gives a path dependent value between s' and s.

$$\epsilon_\eta(s' \to s) = 1 - \exp\Big(- \int_{s'}^s \kappa_\eta ds' \Big) \quad (2.7)$$

By using spectral emissivity, one can define total emissivity as the ratio of total intensity to blackbody intensity which is given in Equation 2.8.

$$\epsilon(s' \to s) = \frac{1}{I_b} \int_0^\infty \epsilon_\eta I_{b\eta} d\eta \quad (2.8)$$

Using emissivity, the intensity solution in Equation 2.6 then can be given in more compact form, which is given in Equation 2.9.

$$I(s) = \Big(1 - \epsilon(T_w, 0 \to s) \Big) I_{bw} - \int_0^s \frac{\partial \epsilon}{\partial s'} \Big(T(s'), s' \to s \Big) I_b(s') ds' \quad (2.9)$$

The net radiative heat flux from a surface along direction $\vec{s}$ is given as

$$\vec{q_\eta} = \int_{4\pi} I_\eta(\vec{s})\vec{n} \cdot \vec{s} d\Omega \tag{2.10}$$

Then total radiative heat flux at a surface is given as

$$\vec{q} = \int_0^\infty \vec{q_\eta} d\eta \tag{2.11}$$

2.3. Gray Model

The gray gas model is first proposed by Hottel who provides very useful charts to calculate emissivity of a gas at varying conditions [13,14]. The data used by Hottel yield large errors at elevated temperatures, and further developments are done by Leckner [15]. In gray gas assumption, absorption and scattering coefficients are independent of wavelength. In other words, the RTE is written for the total radiative intensity and spectral dependency is dropped out in RTE. Because $\kappa_\eta = \kappa$ in gray gas model, spectral emissivity in Equation 2.7 will simply equal to total emissivity, such as

$$\epsilon(T, 0 \to s) = 1 - e^{-\kappa s} \tag{2.12}$$

Total emissivities in gray gas model can be calculated for various gas molecules. For example, the emissivity of the gas mixture of H_2O and CO_2 can be calculated as

$$\begin{aligned}\epsilon = {} & C_{H2O}(p, p_{H2O}, L)\epsilon_{H2O}(T, p_{H2O}, L) \\ & + C_{CO2}(p, p_{CO2}, L)\epsilon_{CO2}(T, p_{CO2}, L) - \Delta\epsilon(T, p_{CO2}, p_{H2O}, L)\end{aligned} \tag{2.13}$$

where C_{H2O} and C_{CO2} are the pressure correction, ϵ_{H2O} and ϵ_{H2O} are emissivity for H_2O and CO_2 respectively, $\Delta\epsilon$ is the mixture correction factor. These parameters can be obtained from Hottel's charts; but, the data is dated back to 1954, so that more recent data such as in [15], should be used. The accuracy of gray models are lately

discussed by Wang et al. [16].

2.4. Spectral Models

An opaque wall can be treated as gray which will be a very simple model to diffuse emission, absorption and reflection. However, considering molecular gases, gray assumption will not be an accurate model to define hot gases behavior at different wavelengths. Therefore, non-gray models to formulate spectral dependency of radiative transfer equation have been developed with increasing knowledge of spectral properties. A line gives the information of wavelength dependent radiative property. The most accurate calculation method is line-by-line in which measured line values used directly in the calculations; however it is the most time consuming and computationally expensive. Apart from the line-by-line calculations, the spectral models may roughly be classified into narrowband, wideband and global models.

In band based models including narrow band, wide band and k-distribution, radiative quantities are calculated between certain intervals (i.e. 25 cm^{-1} or less bandwidth gives higher accuracy results for narrow band modeling) and they can be added together to obtain total results. Narrow band modeling takes advantage of using constant spectral blackbody intensity or Planck function, $I_{b\eta}$ within the band. If a bandwidth is chosen narrow enough, Plank function can be assumed as constant and then averaged values (i.e. absorption coefficient or transmissivity) can be computed for the band. Elsasser [19] and Goody models are proposed to utilize this idea, which are originated in atmospheric sciences where the temperature difference is not more than 320 K and change in pressure is very substantial. The importance of extremely weak lines especially at elevated temperatures is recognized by Malkmus [20]. Including these lines, band models are also used in high temperature radiative heat transfer calculations.

Global models, on the other hand, aim to calculate total radiative heat flux or its divergence directly. These models need spectrally integrated radiative properties such as emissivity. Mean beam length and the weighted sum of gray gases methods which are proposed by Hottel [13] are the earliest of these models and became successful

for determination of radiative heat flux of combustion gases from isothermal medium to cold enclosing walls. The details of these methods are given by Hottel [13] and by Hottel and Sarofim [17] and also in textbooks [1,10]. Recently, full-spectrum correlated k-distributions are also studied [18].

One of the most successful non-gray models is weighted sum of gray gases (WSGG) which is proposed by Hottel [13] first, and then many developments are done [21–23]. In WSGG model, total emissivity in Equation 2.8 is approximated by changing the integral over wave number with summation of J number of gray gases. Total emissivity in WSGG can be calculated as

$$\epsilon(s) = \sum_{j=1}^{J} a_j (1 - e^{-\kappa_j s}) \tag{2.14}$$

where a_j is the weight factor and κ_j is gray gas coefficient. a_j may depend on the source temperature and path, while κ_j is taken as constant. The radiative intensity in Equation 2.9 can be calculated by using WSGG which is given in Equation 2.15.

$$I_j(s) = a_j(T_w) e^{-\kappa_j s} I_{bw} + \int_0^s a_j(s') \kappa_j e^{-\kappa_j [s-s']} I_b(s') ds' \tag{2.15}$$

Setting

$$I(s) = \sum_{j=0}^{J} I_j(s) \tag{2.16}$$

I_j will satisfy radiative transfer equation as

$$\frac{dI_j}{ds} = \kappa_j (a_j I_b - I_j) \tag{2.17}$$

which subjects to boundary condition at $s = 0$

$$I_j = a_j(T_w) I_b(T_w) \tag{2.18}$$

In this work, spectral models are limited to narrowband based k-distributions. Statistical narrow band is the main model which takes into account spectral dependencies of gases with LBL accuracy. Mathematical expressions of k-distributions, cumulative distributions, narrow band data generation, correlated-k assumption are discussed in detail next.

2.4.1. Narrow Band k-Distributions

Absorption coefficient of a participating gas depends on wave number. Under varying conditions such as extremely high temperatures and low pressures, absorption coefficient becomes erratic. To show the effect of temperature and pressure, the absorption coefficient of CO_2 in air against wave number at two temperature and pressure levels are illustrated in Figure 2.4, which has 1500 lines from HITEMP database between wave numbers 2320 and 2330. Three cases shown on the figure are for (300 K - 10 mbar), (300 K - 1 bar) and (1000 K - 1 bar). In the first figure, the medium is at low pressure and low temperature in which absorption coefficient acts like individual lines across spectrum. The reason can be given as that no broadening mechanism is dominant for low pressure and low temperature cases. The middle and bottom figures show that broadening mechanism becomes more active at high pressures and lines are started to be overlapped; however same values of absorption coefficients are still repeatedly occurring at different spectral positions. While working with large spectral ranges, same value of absorption coefficient appears at different wave numbers. In order to avoid solving radiative transfer equation (see Equation 2.3) for the same absorption coefficient, a reordering concept is proposed by Lacis et al. [4] which gives absorption coefficient distribution, namely k-distributions in terms of how many times same value exists at different wave numbers.

2.4.2. Distribution function

Distribution function represents the fraction of spectral regions where absorption coefficient is between κ and $\kappa + \Delta\kappa$. Resulting value of $f(k)$ is normalized to 1 which gives the ratio of total projected length of $\Delta\kappa$ on wave number axis to wave number

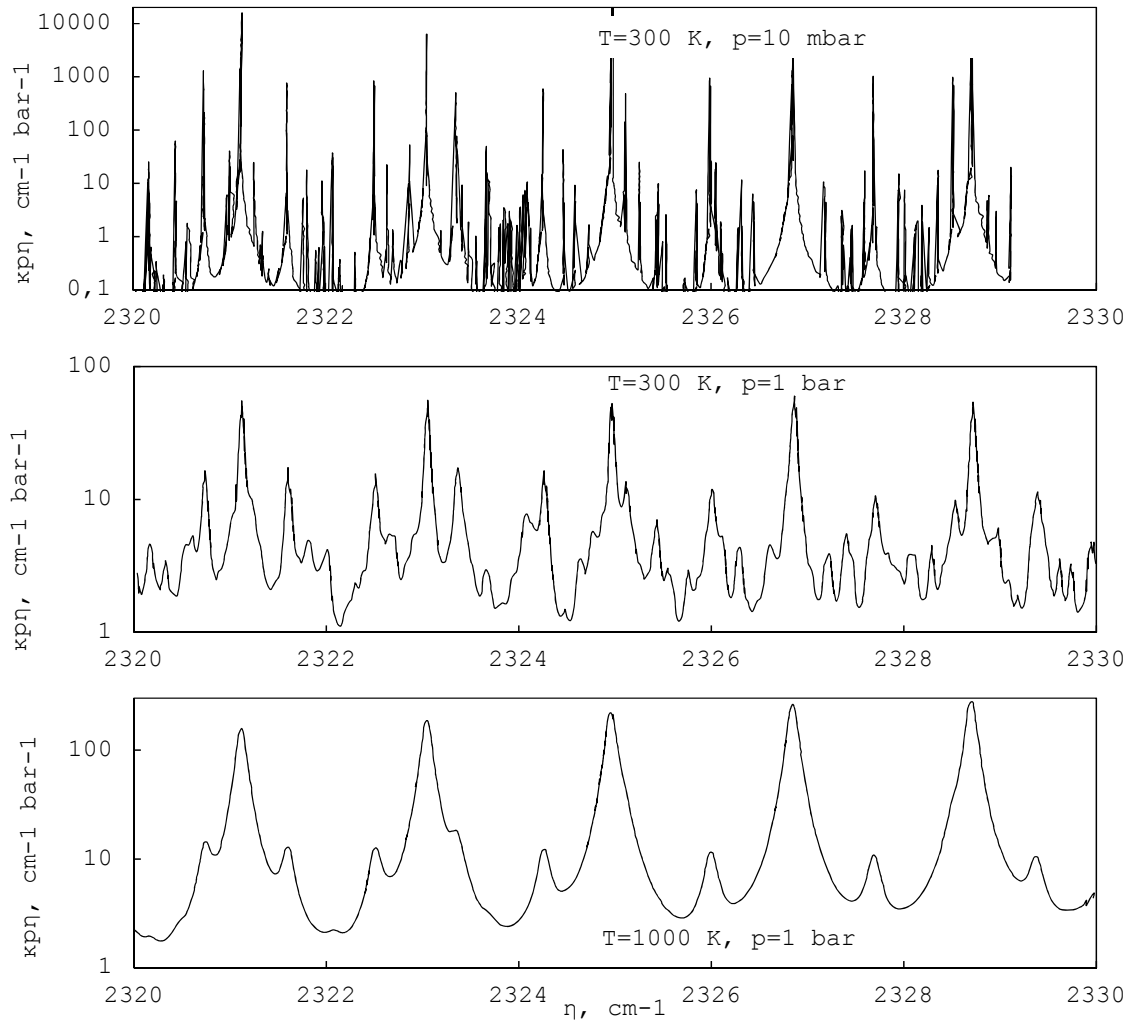

Figure 2.4: Absorption coefficient of small portion of CO_2 in air under various conditions [1].

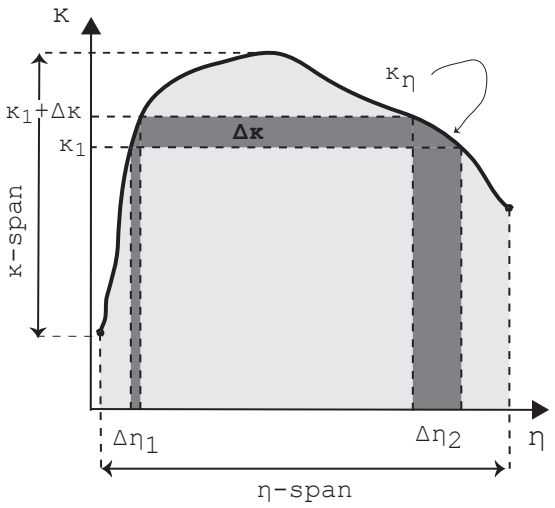

Figure 2.5: Spectral absorption coefficient against wave number. A sample calculation of distribution function of κ_1.

span. In Figure 2.5, sample calculation of the distribution function of k_1 is shown. One can observe that $f(k_1) = (\Delta\eta_1 + \Delta\eta_2)/(\eta - span)$. Same calculation can be done for all κ's in κ-span.

Distribution function (not normalized) is mathematically expressed in Equation 2.19.

$$\bar{f}(k) = \frac{1}{\Delta\eta} \sum_j \left| \frac{d\eta}{d\kappa} \right|_j \tag{2.19}$$

In Equation 2.19, summation over a band $\Delta\eta$ is simply done by dividing κ span into bins numerating each κ intersection like $j = 1, 2, 3...$ and calculating $d\eta/d\kappa$. For each point, $d\eta/d\kappa$ is computed with an absolute sign to maintain that the direction of integration is always from $\kappa_{\eta,min}$ to $\kappa_{\eta,max}$. Distribution function should satisfy the normalization condition which is given in Equation 2.20.

$$\int_0^\infty f(k)dk = 1 \tag{2.20}$$

Distribution function is expressed in a more mathematically refined way in Equation

2.21.

$$f(k) = \frac{1}{\Delta\eta} \int_{\Delta\eta} \delta(k - \kappa_\eta) d\eta \tag{2.21}$$

where $\delta(k - \kappa_\eta)$ is *Dirac-delta function* defined by

$$\int_{-\infty}^{\infty} \delta(k) dk = 1$$

A sample calculation of how distribution function is calculated is shown in Figure 2.6. Absorption coefficient of a small portion of CO_2 with a total pressure of 1 bar is given between wave numbers of 660 and 665 cm^{-1}. The line $\kappa_\eta = 1$ is plotted on the left figure where six intersections with absorption curve are observed. On the right figure, corresponding $f(k)$ can be read. The distribution function is not smooth at all such as there are local minimums and maximums in k. At these points where $d\kappa_\eta/d\eta$ goes zero, $f(k)$ goes infinity which makes integration of distribution function harder in further calculations.

In order to avoid such difficulties, a cumulative function $g(k)$ is introduced. The cumulative function simply sums distribution function along the k-axis. It can be written as,

$$g(k) \equiv \int_0^k f(k) dk \tag{2.22}$$

where g is a value of normalized wave number varying from 0 to 1. The dashed line in Figure 2.6 represents cumulative function of $f(k)$.

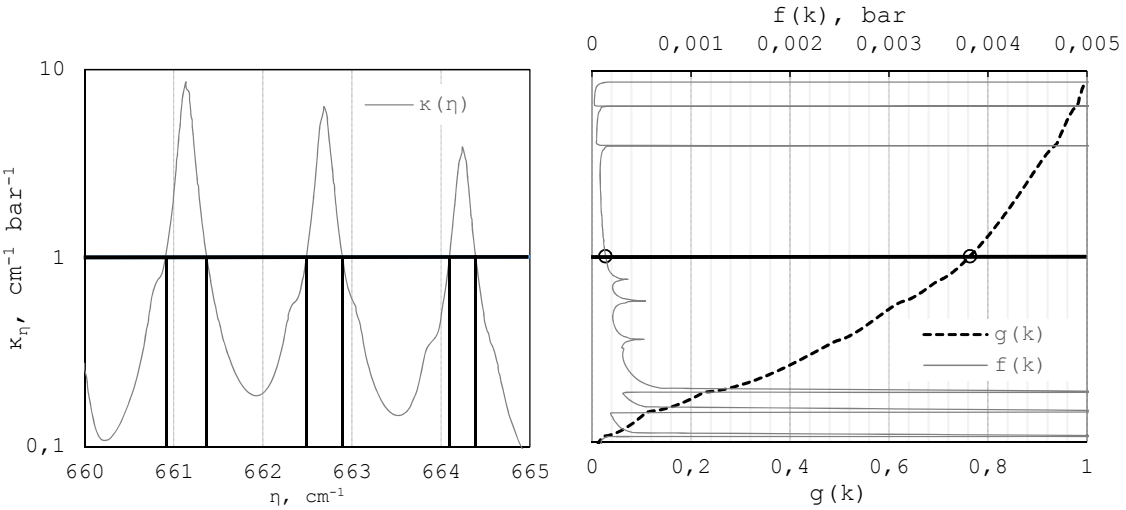

Figure 2.6: Extraction of distribution and cumulative functions of CO_2 (T=296 K and p=1.0 bar) [1].

2.4.3. Implementation of k-distributions

Starting with the definition of averaged transmissivity along a given homogeneous path which is illustrated in Figure 2.3 as

$$\bar{\tau}_\eta(s) = \frac{1}{\Delta\eta}\int_{\Delta\eta} \exp(-\kappa_\eta s)d\eta \tag{2.23}$$

One may substitute distribution function, Equation 2.19, into transmissivity and change order of integration variable from η to κ.

$$\bar{\tau}_\eta(s) = \int_{\kappa_{\eta,min}}^{\kappa_{\eta,max}} \exp(-\kappa_\eta s)\left|\frac{d\eta}{d\kappa_\eta}\right| d\kappa_\eta = \int_0^\infty exp(-ks)f(k)dk \tag{2.24}$$

Application of g(k) into transmissivity can be done in such a way that,

$$\bar{\tau}_\eta(s) = \int_0^\infty \exp(-ks)f(k)dk = \int_0^1 \exp(-k(g)s)dg \tag{2.25}$$

where $k(g)$ is the inverse function of $g(k)$. In Equation 2.25, κ_η is eventually changed with a pseudo absorption coefficient - k which depends on the normalized wave number

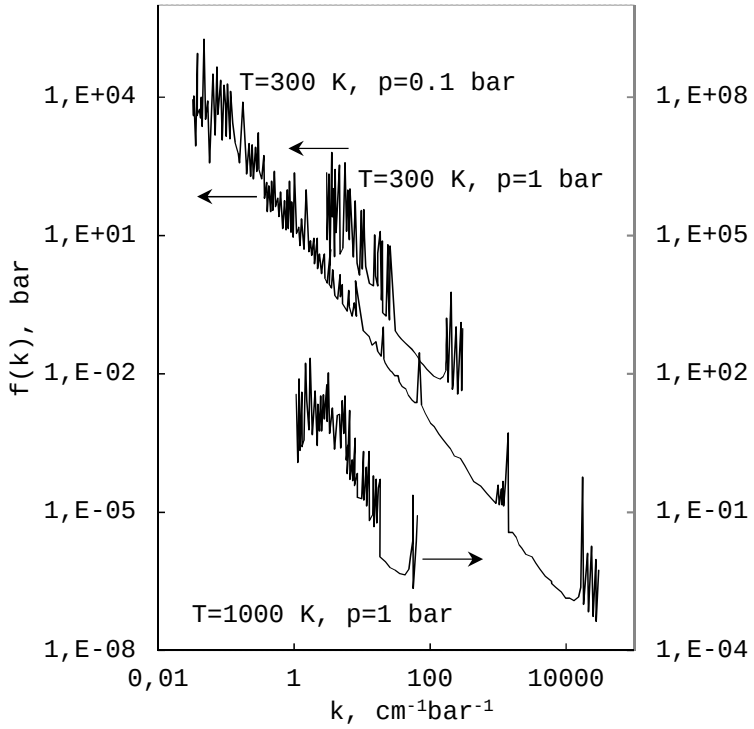

Figure 2.7: Distribution function of CO_2 which is illustrated in Figure 2.4 [1].

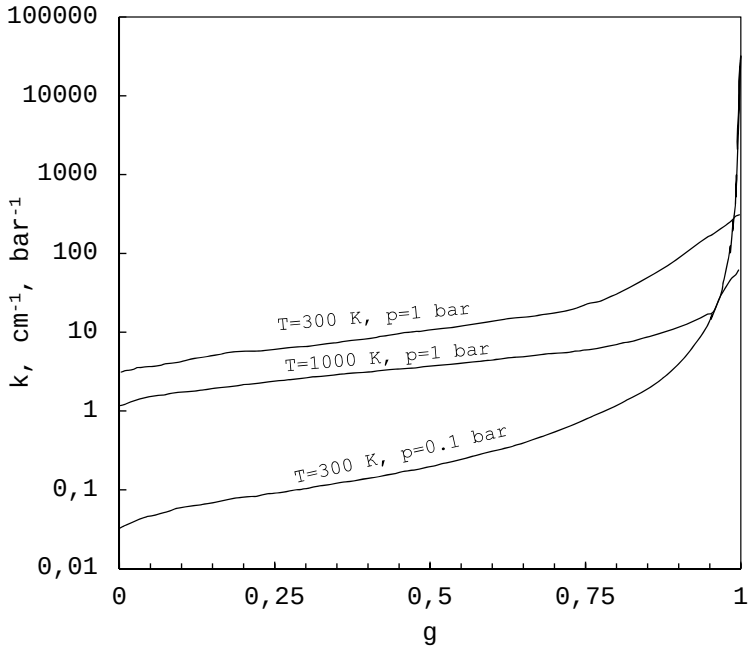

Figure 2.8: Cumulative distribution function of CO_2 which is illustrated in Figure 2.4 [1].

g. Cumulative distribution function is smooth so that Equation 2.25 can be integrated in a more easier way which can be seen by comparing Figures 2.7 and 2.8. At this point, $k(g)$ is required in radiative calculations instead of $g(k)$. For that reason, $k(g)$ should be found by using a method to find inverse of a function such as bisection method. Extraction of $g(k)$ data like in Figure 2.6 is done by putting Equation 2.21 into the definition of $g(k)$ will lead to,

$$g(k) = \int_0^k f(k)dk = \frac{1}{\Delta\eta}\int_{\Delta\eta}\int_0^k \delta(k-\kappa_\eta)dkd\eta = \frac{1}{\Delta\eta}\int_{\Delta\eta} H(k-\kappa_\eta)d\eta \qquad (2.26)$$

where $H(k)$ is Heaviside's unit step function.

$$H(k) = \begin{cases} 0, & k < 0, \\ 1, & k > 0. \end{cases}$$

2.4.4. Scaled-k and correlated-k assumptions

Applying k-distributions to a non-homogeneous medium requires additional assumptions. There are mainly two approximations. First one is scaled-k in which absorption coefficient is written as product of two functions that represent wave number and location dependencies showed in Equation 2.27.

$$\kappa_\eta(\eta, T, p, p_a) = k(\eta)u(T, p, p_a) \qquad (2.27)$$

In above equation, absorption coefficient at any state is separated into two functions k and u. The first function k depends only on wave number while function u depend on temperature, total and partial pressures.

In correlated-k method, by knowing $k(g)$ for specific states, the same value of g at different locations can be mapped into different k values. If k-distribution is in the narrow band or variation in Planck function is negligible, then we are able to construct correlated-k model in absorption coefficient estimations. We can write "correlated"

k-distributions with a good accuracy in Equation 2.28.

$$\bar{\tau}_\eta(0 \to s) = \frac{1}{\Delta\eta} \int_{\Delta\eta} \exp\left(-\int_0^s \kappa_\eta ds'\right) d\eta \cong \int_0^1 \exp\left(-\int_0^s k(s', g) ds'\right) dg \quad (2.28)$$

If averaged transmissivity is considered in a non-homogeneous medium, correlated-k model enables us to express radiative properties using advantages of k-distribution. Integral over s meaning that transmissivity is calculated starting from leaving point 0 and integrating along a column of non-homogeneous path which is illustrated in Figure 2.3. The advantages and drawbacks of these assumptions given in [5].

2.4.5. Statistical Narrowband Correlated-k Model (SNBCK)

Statistical narrowband correlated-k model (SNBCK) is first proposed by Lacis and Oinas [4] and Goody [24] in order to be used in atmospheric radiation calculations which are limited to model one dimensional atmospheric layers. Afterwards, some efforts have been made by Lui *et al.* [25] to adapt and to develop the SNBCK model in thermal radiative transfer. Narrowband gas transmissivity is given by Malkmus [26] as

$$\bar{\tau}_\eta(L) = \exp\left(-\frac{\pi B}{2}\left(\sqrt{1 + \frac{4SL}{\pi B}} - 1\right)\right) \quad (2.29)$$

where

$$B = \frac{2\bar{\beta}_v}{\pi^2},\ S = \bar{k}_v X p,\ \bar{\beta}_v = 2\pi\bar{\gamma}_v/\bar{\delta}_v. \quad (2.30)$$

X is the molar fraction of radiating gas, L is gas column length and p is the total pressure. $\bar{k}_v$, $\bar{\gamma}_v$ and $\bar{\delta}_v$ are band parameters which have their usual meanings such as mean line intensity to line spacing ratio, average line Lorentz half-width, and mean line spacing in the same order.

A narrowband database has been made available including $\bar{k}_v$ and $\bar{\delta}_v$ parameters

by Soufiani and Taine [27]. Because $\bar{\delta}_v$ is not directly used in SNBCK model, values of $1/\bar{\delta}_v$ are tabulated in the database. $\bar{k}_v$ and $1/\bar{\delta}_v$ are given in files SNBH2O and SNBCO2 from under the acronym EM2C [27] for temperatures between 300 K and 2900 K with at 14 distinct temperatures with a 25 cm^{-1} spectral resolution. For H_2O, the parameters are given for bands centered at a wave number ranging continuously from 150 cm^{-1} to 9300 cm^{-1} (367 bands). For CO_2, the parameters are not given in the transparency regions. The centers of the contributing bands range from 450 to 1200 cm^{-1} (31 bands), from 1950 to 2450 cm^{-1} (21 bands), from 3300 to 3800 cm^{-1} (21 bands) and from 4700 to 5250 cm^{-1} (23 bands). The total number of CO_2 bands is 96. $\bar{\gamma}_v$ is a typical collisional half-width of the lines of the absorbing gas which is given in the study of Soufiani and Taine [27] as

$$\bar{\gamma}_{H_2O} = \frac{p}{p_s}\left[\frac{T_s}{T}0.462X_{H_2O} + \left(\frac{T_s}{T}\right)^{0.5}(0.0792(1-X_{CO_2}-X_{O_2})+0.106X_{CO_2}+0.036X_{O_2})\right] \quad (2.31)$$

$$\bar{\gamma}_{CO_2} = \frac{p}{p_s}\left(\frac{T_s}{T}\right)^{0.7}\left(0.07X_{CO_2}+0.058(1-X_{CO_2}-X_{O_2})+0.1X_{O_2}\right) \quad (2.32)$$

where T_s is 296 K, p_s is 1 atm and X is molar fraction of corresponding species.

2.4.6. Distribution and cumulative functions in SNBCK

Domoto [28] introduced distribution function in SNBCK by taking the inverse Laplace transformation of statistical narrow band transmissivity which is given in Equation 2.29 as

$$f(k) = 0.5k^{-3/2}(BS)^{0.5}\exp\left(\frac{\pi B}{4}(2-S/k-k/S)\right) \quad (2.33)$$

Then, cumulative function is found in same manner as,

$$g(k) = 0.5\Big(1 - erf(a/\sqrt{k} - b\sqrt{k})\Big) + 0.5\Big(1 - erf(a/\sqrt{k} + b\sqrt{k})\Big)e^{\pi B} \tag{2.34}$$

where $a = \sqrt{\pi BS}/2$, $b = \sqrt{\pi B/S}/2$ and erf(x) is the error function which is given as erf$(x) = \frac{2}{\sqrt{\pi}} \int_0^x \exp(-t^2)dt$.

2.5. Radiative Transfer Equation - Numerical Solution

Radiative heat transfer equation is an integro-differential equation, its exact solution is only available for very specific cases (i.e. one dimensional and only absorbing and emitting). When the case is defined in multi-dimensional environment and/or included scattering effects, the solution to the radiative heat transfer should be numerically obtained. Many methods have been developed such as moment method, spherical harmonics, discrete ordinates, zonal method and Monte Carlo [1]. Among them, discrete ordinates method is one of popular ones that solves radiative transfer equation for a set of n different angles called ordinates.

2.5.1. Discrete Ordinates Method

In discrete ordinates method, directional dependence of RTE is replaced with numerical quadratures for an arbitrary direction dependent function $D(\vec{s})$ is given in Equation 2.35, where ω is weight of the numerical quadratures.

$$\int_{4\pi} D(\vec{s})d\Omega \simeq \sum_{m=1}^{N} \omega_m D(\vec{s}_m) \tag{2.35}$$

Applying discrete ordinates to RTE (Equation 2.3) leads to

$$\vec{s}_m \cdot \nabla I_\eta(\vec{s}, \vec{s}_m) = -(\kappa_\eta(\vec{s}) + \sigma_\eta(\vec{s}))I_\eta(\vec{s}, \vec{s}_m) + \kappa_\eta(\vec{s})I_{b\eta}(\vec{s}) + \frac{\sigma_\eta(\vec{s})}{4\pi} \sum_{j=1}^{N} \omega_j I_\eta(\vec{s}, \vec{s}_j)\Phi(\vec{s}, \vec{s}_m, \vec{s}_j) \tag{2.36}$$

Directional integration is dropped and replaced with N number of equations (m=1,2,..N). The boundary condition can also be given in same way

$$I_\eta(\vec{s}_w, \vec{s}_m) = \epsilon_\eta(\vec{s}_w) I_{b\eta}(\vec{s}_w) + \frac{\rho_\eta(\vec{s}_w)}{\pi} \sum_{\vec{n}\cdot\vec{s}_j'<0} \omega_j I(\vec{s}_w, \vec{s}_j)|\vec{n}\cdot\vec{s}_j|,\ \vec{n}\cdot\vec{s}_j > 0. \tag{2.37}$$

Discrete ordinates can be generated if the following zeroth, first and second moments are satisfied [1].

$$\sum_{m=1}^{N} \omega_m = 4\pi;\ \sum_{m=1}^{N} \omega_m \vec{s}_m = 0;\ \sum_{m=1}^{N} \omega_m \vec{s}_m \vec{s}_m = \frac{4\pi}{3}\delta \tag{2.38}$$

where δ is the unit tensor. After satisfying above conditions, we will have set of discrete directions $\vec{s}_m$ such as

$$\vec{s}_m = \xi_m \hat{\mathrm{i}} + \eta_m \hat{\mathrm{j}} + \mu_m \hat{\mathrm{k}}. \tag{2.39}$$

2.5.2. Two dimension and non-scattering assumption

When considering combustion of hydrocarbon fuels, it is assumed that CO_2 and H_2O are the only product gases that are radiating in thermal region of the spectrum. Nitrogen comprises 78% of the atmosphere but actually it is transparent in thermal region. Since these gases are small molecules under or at near atmospheric pressures, their scattering effects are always ignored. It is assumed that the fuel combustion does not generate soot (not valid for all hydrocarbon fuels). So, combustion products can be approximated as absorbing and emitting medium. In addition, two dimension assumption is also taken into consideration in many cases. For example, the rotor axis of a jet engine can be taken as symmetry line or the mass flow direction of a rocket engine. The results may not be so detailed but gives many inside information during modeling process. Thus, writing radiative transfer equation in discrete ordinates for

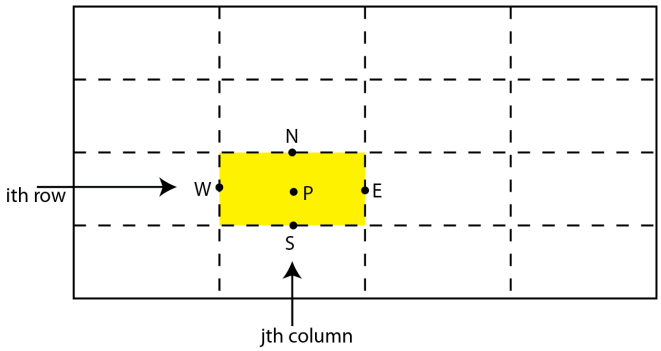

Figure 2.9: Typical control volume.

two dimensional medium leads to [10, 25, 29].

$$\xi_m \frac{\partial I_{\eta,m}}{\partial x} + \eta_m \frac{\partial I_{\eta,m}}{\partial y} = \kappa_\eta I_{b\eta} - \kappa_\eta I_{\eta,m} \tag{2.40}$$

where ξ_m and η_m are the direction cosines of the m^{th} discrete ordinate which is in the direction of $\vec{s}_m$. W_x and W_y are weighting factors that relate wall intensity to cell center intensity such as

$$I_{\eta,m,p} = W_{x,m} I_{\eta,m,e} + (1 - W_{x,m}) I_{\eta,m,w} \tag{2.41}$$

$$I_{\eta,m,p} = W_{y,m} I_{\eta,m,n} + (1 - W_{y,m}) I_{\eta,m,s} \tag{2.42}$$

Total number of unknowns becomes five with these three equations, namely $I_{\eta,n}$, $I_{\eta,w}$, $I_{\eta,s}$, $I_{\eta,e}$ and $I_{\eta,p}$. The solution is only possible if two of them are known. If the ordinate is in north-east direction (see Figure 2.9, then both south and west wall intensities are known during sweeping of the domain along the ordinate, and Equations 2.41 and 2.42 will relate north, and east intensities to the intensity at the nodal point. The intensity at a nodal point P for a control volume (see Figure 2.9) which is in the i^{th} row and j^{th} column of spatially discretized rectangular enclosure can be written as

$$I_{\eta,m,p} = \frac{(\xi_m / W_{x,m}) I_{\eta,m,w} \Delta y + (\eta_m / W_{y,m}) I_{\eta,m,s} \Delta x + \kappa_\eta I_{b\eta,p} \Delta x \Delta y}{(\xi_m / W_{x,m}) \Delta y + (\eta_m / W_{y,m}) \Delta x + \kappa_\eta \Delta x \Delta y} \tag{2.43}$$

where subscripts w and s correspond to west and south wall for upstream spectral wall intensity. A constant value for W_x and W_y can be taken as 0.5 or 1; however it generates oscillating or negative intensity which is not physically possible. To overcome this difficulty, so called "positive scheme" given next is used in this work that is described by Liu et al [25].

$$W_{x,m} = max(0.5, W_{x,m'}) \tag{2.44}$$

$$W_{y,m} = max(0.5, W_{y,m'}) \tag{2.45}$$

where $W_{x,m'} = 1-\alpha/(2\beta+\kappa_\eta)$, $W_{y,m'} = 1-\beta/(2\alpha+\kappa_\eta)$, $\alpha = \xi_m/\Delta x$ and $\beta = \eta_m/\Delta y$.

2.6. Computational Model

Radiative transfer equation for emitting, absorbing and non-scattering medium is given in Equation 2.46 that is solved for every angle and control volume; however, given equation does not take advantage of k-distributions. They can be simply added by changing κ_η with $k(g)$. The equation and its solution are given as follows.

$$\xi_m \frac{\partial I_{\eta,m}}{\partial x} + \eta_m \frac{\partial I_{\eta,m}}{\partial y} = -k_\eta I_{b\eta} - k_\eta I_{\eta,m} \tag{2.46}$$

$$I_{\Delta\eta,m,p,i} = \frac{(\xi_m/W_{x,m})I_{\Delta\eta,m,w}\Delta y + (\eta_m/W_{y,m})I_{\Delta\eta,m,s}\Delta x + k_{\Delta\eta,i}I_{b\Delta\eta,p}\Delta x\Delta y}{(\xi_m/W_{x,m})\Delta y + (\eta_m/W_{y,m})\Delta x + k_{\Delta\eta,i}\Delta x\Delta y} \tag{2.47}$$

where $\Delta\eta$ meaning that all calculations will be done for each narrowband. Ordinates are specified by using T_7 angle scheme which is one of the most successful angular discretization schemes and it is provided by Thurgood [30]. It is consisting of 196 (m=1,2,3...196) discrete angles. Angle sets are given in the appendix. Only positive values are provided; however the other directions can be found from the relations: $\vec{s}_m = -\xi_m\hat{\imath} + \eta_m\hat{\jmath}$, $\vec{s}_m = -\xi_m\hat{\imath} - \eta_m\hat{\jmath}$ and $\vec{s}_m = \xi_m\hat{\imath} - \eta_m\hat{\jmath}$.

Table 2.1: The 7-point Gauss-Lobatto quadrature scheme.

i	g_i	w_i
1	0.00000	0.04500
2	0.15541	0.24500
3	0.45000	0.32000
4	0.74459	0.24500
5	0.90000	0.05125
6	0.93551	0.05125
7	0.98449	0.03764

In order to obtain $k_{\Delta\eta,i}$, narrowband averaged cumulative distribution function $g(k)$ is inverted to get $k(g)$. Using 7-point Gauss-Lobatto quadrature scheme, k_i values at corresponding g_i are found by bisection method. The algorithm of finding roots of $g(k)$ using bisection method is given in Figure 2.11. The points and weights of 7-point Gauss-Lobatto scheme are given in Table 2.1. k-distributions of 1% CO_2 in N_2 is calculated for narrowbands namely, 2250, 2275, 2300 and 2325 cm^{-1} at points given in Gauss-Lobatto scheme. They are plotted in Figure 2.10.

2.6.1. Spectral Blackbody Emissive Intensity

The term $I_{b\Delta\eta,p}$ in Equation 2.47 is spectral blackbody emissive intensity within a narrowband which depends on cell temperature T and the narrow band position in the spectrum. If η_1 and η_2 are initial and final wave numbers, then $I_{b\Delta\eta,p}$ can be calculated as [1],

$$I_{b\Delta\eta} = \frac{C_1 T^4}{C_2 \pi} \int_{C_2\eta_2/T}^{C_2\eta_1/T} \frac{\xi^3 d\xi}{\exp(\xi) - 1} \tag{2.48}$$

where C_1 and C_2 are radiation constants given as $3.7418 \cdot 10^{-16}\ Wm^2$ and $1.4388\ cmK$ correspondingly. A code is written in order to find blackbody intensity between wave numbers 150 - 9300 cm^{-1} with a narrowband interval of 25 cm^{-1} and between temperatures 300 - 2700 K with an increment of 100 K. The algorithm of the code used to

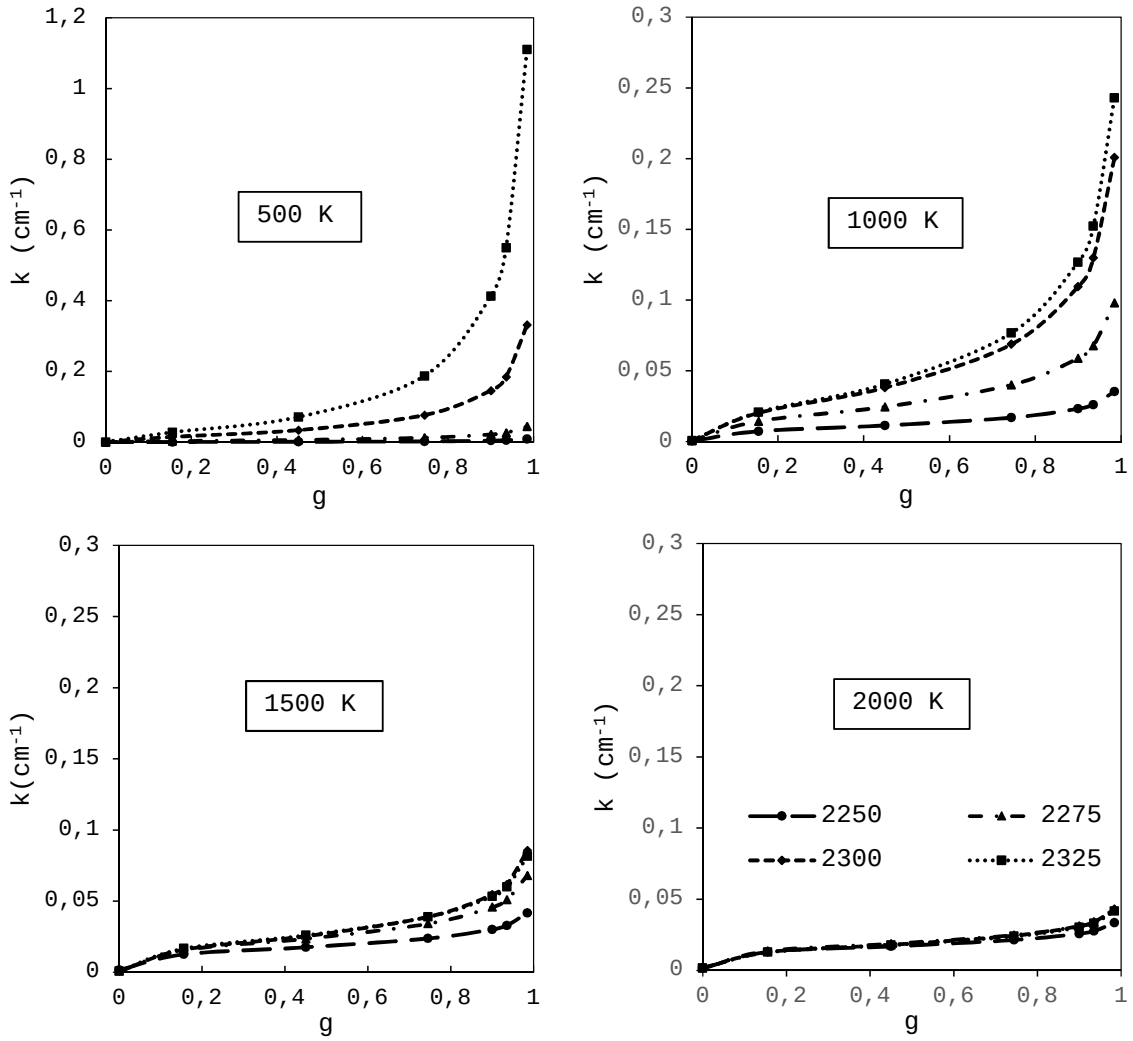

Figure 2.10: Absorption coefficients are plotted against cumulative distribution function within narrowbands at 2250, 2275, 2300, 2325 cm^{-1} and at temperatures 500, 1000, 1500, 2000 K.

Kappa;
input : Temperature, Pressure, X_{CO2}, X_{H2O}
output: $k_{CO2}(g)$, $k_{H2O}(g)$

find B_{CO2}, S_{CO2}, B_{H2O}, S_{H2O} using Equation 2.30;
find γ_{CO2}, γ_{H2O} using Equation 2.32 and (2.31;
for *i=1 to 7 Quadrature Points (Table 2.1)* **do**
  for *j=1 to 96 CO_2 Narrowbands* **do**
    find $k_{CO2}(i,j)$ using Equation 2.34;
  end
  for *j=1 to 367 H_2O Narrowbands* **do**
    find $k_{H2O}(i,j)$ using Equation 2.34
  end
end

Figure 2.11: Algorithm: Kappa.

calculate blackbody emissions is given in Figure 2.12.

2.6.2. Overlapping Bands

Numerical calculations are done according to whether bands are overlapping or not. For those 96 CO_2 narrowbands, wave number ranges from 450 to 1200 cm^{-1} (31 bands), from 1950 to 2450 cm^{-1} (21 bands), from 3300 to 3800 cm^{-1} (21 bands) and from 4700 to 5250 cm^{-1} (23 bands), H_2O is also active between wave numbers 150 - 9300 cm^{-1} (367 bands). The overlapping bands are shown in Figure 2.13. For that reason, overlapping treatment should be employed before going any further. At any overlapping band, $k(g)$ values are found simply adding $k(g)$ values is shown in radiative transfer equation as follows.

$$\xi\frac{\partial I_{ij}}{\partial x}+\eta\frac{\partial I_{ij}}{\partial y}=(k_{CO2,i}+k_{H2O,j})I_b-(k_{CO2,i}+k_{H2O,j})I_{ij} \tag{2.49}$$

Blackbody;

input* : *finds find spectral blackbody emissions;

input : T,$\Delta\eta$

output: $I_b(\Delta\eta,T)$

for *i=1 to 367 Narrowbands* **do**

  for *j=1 to 25 Temperatures* **do**

    find $I_b(i,j)$ using Equation 2.48;

  end

end

Figure 2.12: Algorithm: Blackbody.

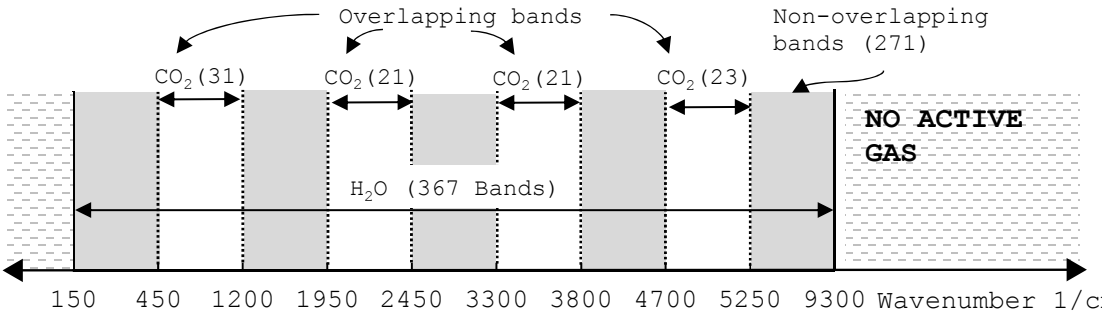

Figure 2.13: All active bands. Number of overlapping and nonoverlapping bands are given. The regions where wave number less than 150 and greater than 9300 cm^{-1} are not thermally active.

Intensity at a nodal point is given as

$$I_{\Delta\eta,m,p} = \sum_{i=1}^{7}\sum_{j=1}^{7} w_i w_j I_{\Delta\eta,m,p,ij} \tag{2.50}$$

where i=1,2..7 and j=1,2..7 are quadrature points. Notice that if the band is not an overlapping one Equation 2.51 is used instead of Equation 2.50.

2.6.3. Radiative Spectral Intensity and Flux

By numerically having blackbody intensity and k-distributions of CO_2 and H_2O, Equation 2.47 can be solved for given temperature and molar concentration fields of CO_2 and H_2O. Once radiative intensity for every point of quadrature scheme is obtained, the spectral intensity at a nodal point can be found by

$$I_{\Delta\eta,m,p} = \sum_{i=1}^{7} w_i I_{\Delta\eta,m,p,i} \tag{2.51}$$

Spectral radiative intensity field is calculated by using heat flux definition in Equation 2.10, as an example radiative heat flux in the east direction is given in discrete ordinates as follows.

$$\vec{q}_{\Delta\eta,e} = \sum_{m=1}^{196} \xi_m I_{\Delta\eta,e}\omega_m \tag{2.52}$$

Spectral divergence of heat flux or radiation source term at the point p can then be calculated as

$$\vec{\nabla}\cdot\vec{q}_{\Delta\eta,p} = \left(\frac{\vec{q}_{\Delta\eta,e} - \vec{q}_{\Delta\eta,w}}{\Delta x} + \frac{\vec{q}_{\Delta\eta,n} - \vec{q}_{\Delta\eta,s}}{\Delta y}\right) \tag{2.53}$$

2.6.4. Total Intensity and Flux

Total narrowband averaged intensity is given in Equation 2.51, by using summation over discrete angles, spectral intensity from all directions as

$$I_{\Delta\eta,p} = \sum_{m=1}^{196} \omega_m I_{\Delta\eta,m,p} \tag{2.54}$$

Then, total intensity at a point can be found by summation over all narrowbands as

$$I_p = \sum_{all\ \Delta\eta} I_{\Delta\eta,p} \tag{2.55}$$

Total heat flux in the east direction are given in Equation 2.56. Total divergence of heat flux can also be found as in Equation 2.57.

$$\vec{q_e} = \sum_{all\ \Delta\eta} \vec{q}_{\Delta\eta,e} \tag{2.56}$$

$$\vec{\nabla} \cdot \vec{q} = \sum_{all\ \Delta\eta} \left(\frac{\vec{q}_{\Delta\eta,e} - \vec{q}_{\Delta\eta,w}}{\Delta x} + \frac{\vec{q}_{\Delta\eta,n} - \vec{q}_{\Delta\eta,s}}{\Delta y} \right) \tag{2.57}$$

2.6.5. Radiation Solver

Radiation model on MATLAB solves radiative transfer equations defined in Equation 2.47, 2.41 and 2.42 using boundary condition of black walls as T_w= 300 K. Resulting intensity then put into the Equation 2.52 and 2.53 in order to find heat flux and their divergence. Basic flowchart sums up whole procedure given in Figure 2.14.

First of all, geometry is defined as rectangular region having side lengths of $X = 1$ and $Y = 0.5$ m. Mesh is consisting of 400 uniform rectangles having side lengths of $\Delta x = 0.05$ and $\Delta y = 0.0025$ m. For each one of 400 cell, a temperature, a molar

fractions of H_2O and CO_2 are obtained from flow solver. Using those cell values, k-distributions are calculated for each species, narrowband (CO_2: 96 and H_2O: 367) and quadrature points. The calculation of $g(k)$ is previously given in Equation 2.34.

Secondly, spectral blackbody emissions are calculated as in Equation 2.48 which depends only on cell temperature. Radiative transfer equation, finally, is solved for every spectral and quadrature points. Using spectral intensity, spectral heat flux and divergence of heat flux are calculated according to Equations 2.52 and 2.53. The verification of the solver is done for six cases which is the topic of next section. And later, a sample calculation is done and its solution is presented in Section 4.

2.7. Validation

Current model, named 2drte, of non-gray radiative heat transfer is tested under a constant absorption coefficient case and five inhomogeneous cases. The cases were used by Goutiere et.al [9] comparing five different models of non-gray gases. All cases are enclosed by cold and black walls and medium is at a uniform total pressure of 1 atm having dimensions of 1 m in x-direction, 0.5 m in y-direction. The mesh size is selected as the same as in Goutiere's work as 21-by-21 for all test cases. Grid dependency of the radiation solver is tested with 41-by-41 and 61-by-61 mesh sizes, and the solutions are shown to be grid independent. First of all, a constant absorption coefficient test is carried out in order to show that discrete ordinates method is working properly. After constant absorption coefficient test, the actual five cases are tested which are having non-gray characteristics. In first four cases, single radiating gas (H_2O or CO_2) is modeled while in case five, specific amounts of molar fraction of CO_2 and H_2O are prescribed. Following equations describe the temperature and molar fraction of each case.

$$T(x,y) = T_0\Big(0.3333(1-2|x-0.5|)(1-4|y-0.25|)+1\Big) \tag{2.58}$$

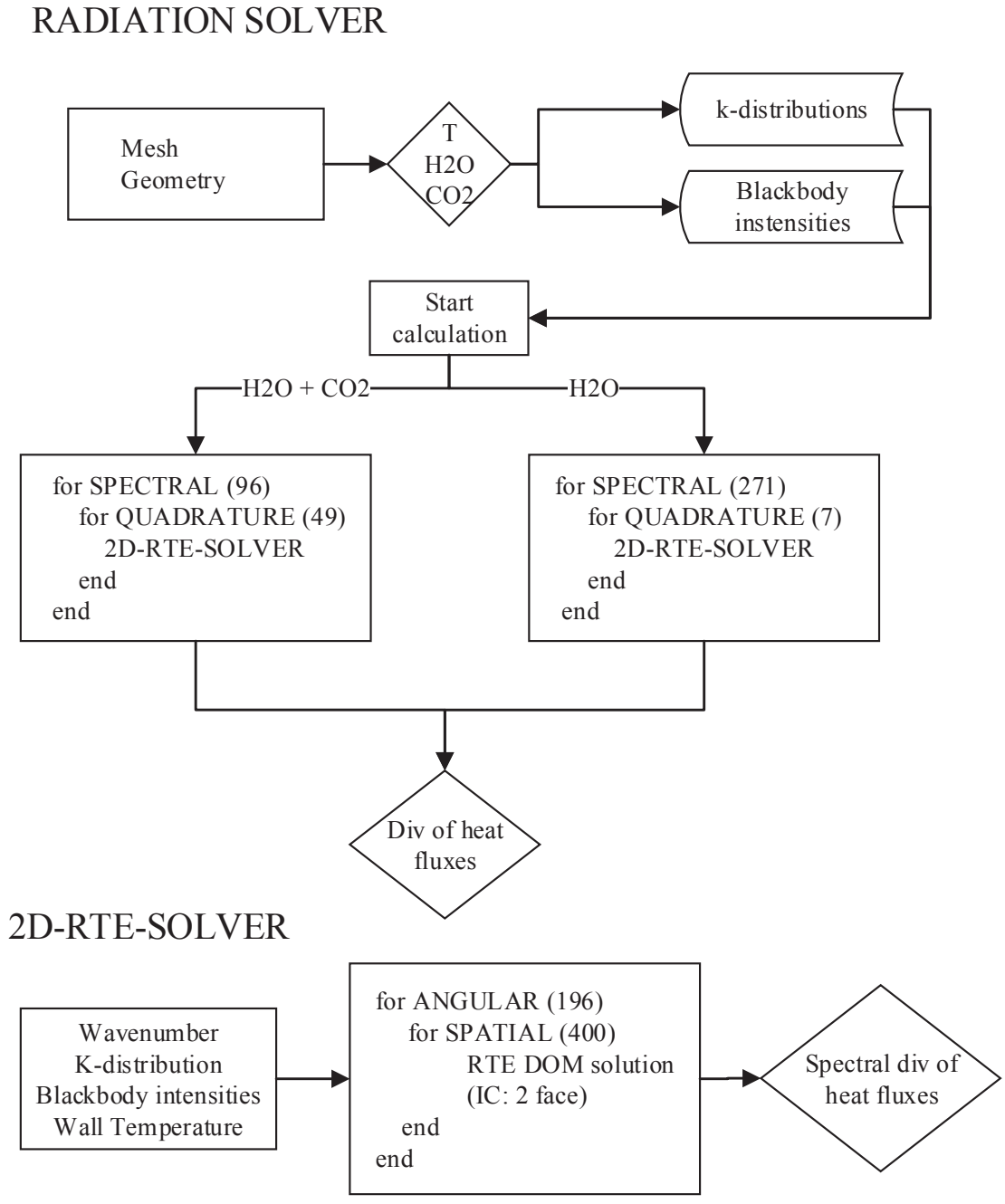

Figure 2.14: Flow chart of RTE Solver.

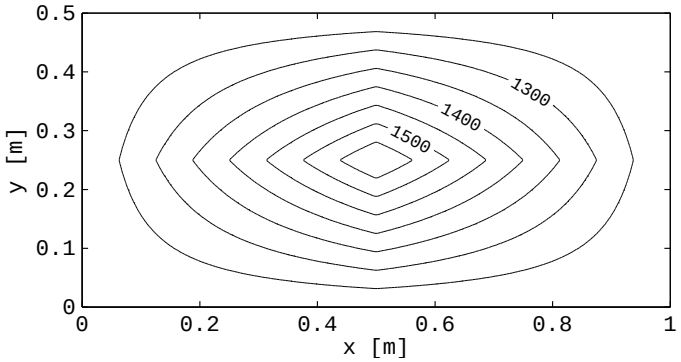

Figure 2.15: Temperature distribution for case two and four. The difference between lines is 50 K.

Table 2.2: Summary of cases tested.

Case	Radiating Gas	Temperature	Mole Fraction
0	$\kappa_\eta = 0.5$	Isothermal: 1000K	-
1	CO_2	Isothermal: 1000K	10%
2	CO_2	Non-isothermal: Eq.2.58	Eq.2.59
3	H_2O	Isothermal: 1000K	20%
4	H_2O	Non-isothermal: Eq.2.58	Eq.2.59
5	CO_2+H_2O	Non-isothermal: Eq.2.60	10% CO_2 + 20%H_2O

$$c(x,y) = c_0\Big(4(1-2|x-0.5|)(1-4|y-0.25|)+1\Big) \tag{2.59}$$

where $To = 1200$ K, c_0 is 0.02 for case two and 0.04 for case four. Equation 2.58 and 2.59 describe the temperature and concentration profiles of case two and four which are given in Figures 2.15, A.3 and A.6. Temperature distribution of case five is given in Equation 2.60 which is also plotted in Figure 2.16. Table 2.2 sums up the cases. In the following section, the solution of and comparison with LBL of case 5 are presented; other cases are given in the appendix.

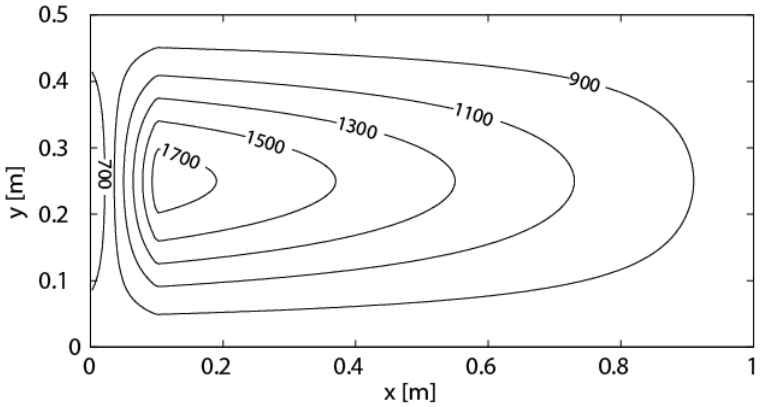

Figure 2.16: Temperature distribution for case five [K].

2.7.1. Case Five

Temperature field of case five has strong inhomogeneities as seen in Figure 2.16. It has high temperature core region exceeding 1600 K and temperature slightly decreases up to 800 K while getting closer to walls. The equation of temperature field is given in Equation 2.60. Molar concentrations of CO_2 and H_2O are kept constant for this case.

for $x \leq$0.1 m

$$T(x,y) = 800 + (14000x - 400)(1 - 3y_0^2 + y_0^3)$$

for $x >$ 0.1 m

$$T(x,y) = 800 - \frac{10000}{9}(x-1)(1 - 3y_0^2 + y_0^3) \tag{2.60}$$

where $y_0 = |0.25 - y|/0.25$.

Divergence of heat flux profiles are plotted in order to compare with line-by-line results. Figure 2.17 shows that current model of radiative heat transfer solves at line-by-line accuracy. At the same time, model can produce wavelength dependent results which means divergence of spectral heat flux can be calculated at any point in the medium (Figure 2.18) i.e. which spectral band contributes most or at which point considered band radiates most. For example, spectral divergence of heat flux

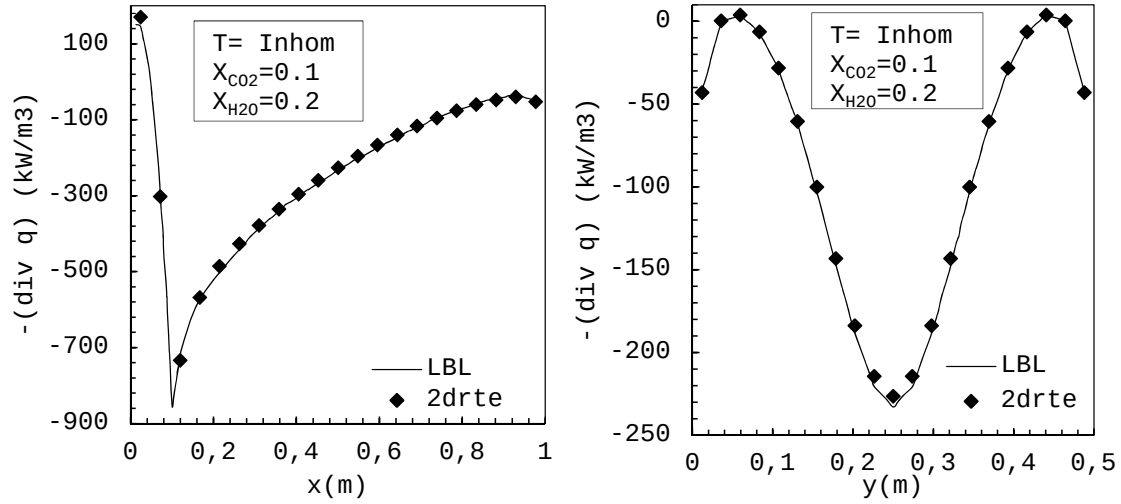

Figure 2.17: Case Five: Distribution of radiative source term along $y = 0.25$ (left) and $x = 0.50$ (right).

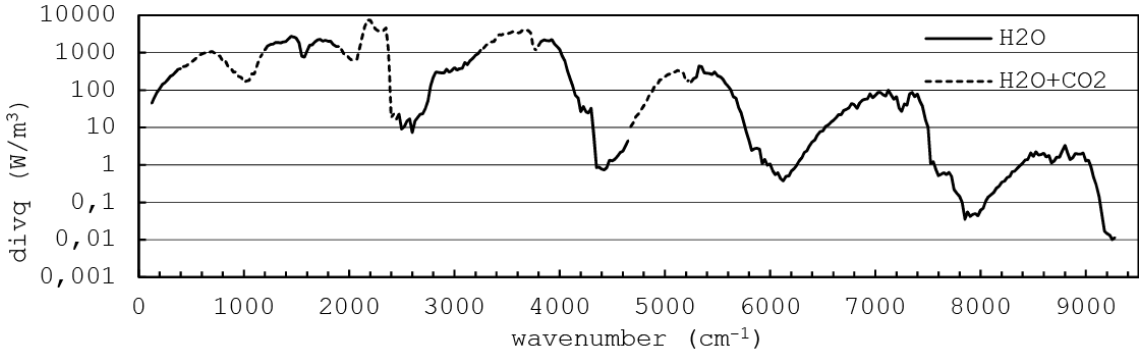

Figure 2.18: Case Five: Divergence of heat flux versus wave number x=0.5 y=0.25.

calculated at the point where x=0.5 and y=0.25 m. In this figure, CO_2 and CO_2 + H_2O radiation can be observed separately for varying narrow bands. It can be seen from this figure that most contributions are done within bands covering 2000 - 2500 and 3000 - 4000 cm^{-1} of order over 1000 W/m^3.

To sum up, current model of radiative heat transfer is tested under six cases. By first one, discrete ordinate method is verified. The other five cases show that current numerical solution of radiative transfer is valid along paths of non-homogeneous temperature and molar fractions for both contributing gases of H_2O and CO_2.

3. FLAME MODEL AND RADIATIVE MODEL COUPLING

A computational model is developed in order to find more accurate solutions to a flame problem in terms of radiative transfer. The solution needs to be line-by-line accurate, but at the same time the computational cost should be decreased. Another reason why a flame model is coupled with the radiation solver is that the spectral wall heat fluxes of a combustion environment will be available.

Flame model is consisting of set of equations, which are equation of turbulent transport, energy and species transport. The flow solver runs in ANSYS Fluent environment and radiative solver runs in MATLAB environment. The data exchange between solvers is established such a way that radiation solver takes temperature and molar concentration fields of CO_2 and H_2O as input, which are the solution of flow solver. The flow solver, on the other hand, takes divergence of heat flux field, which is a term in the energy equation. The model can be described basically in Figure 3.1. A flame is modeled in flow solver, that is in two dimensions and having boundary condition of black walls. The governing equations including continuity (Equation 3.3), momentum (3.4), heat (3.5), k-ε (3.12, 3.13), and species transport (3.14) are solved simultaneously by using the flow solver. The flow parameters including geometry, mesh size, input values of velocities, temperatures, concentrations and turbulent

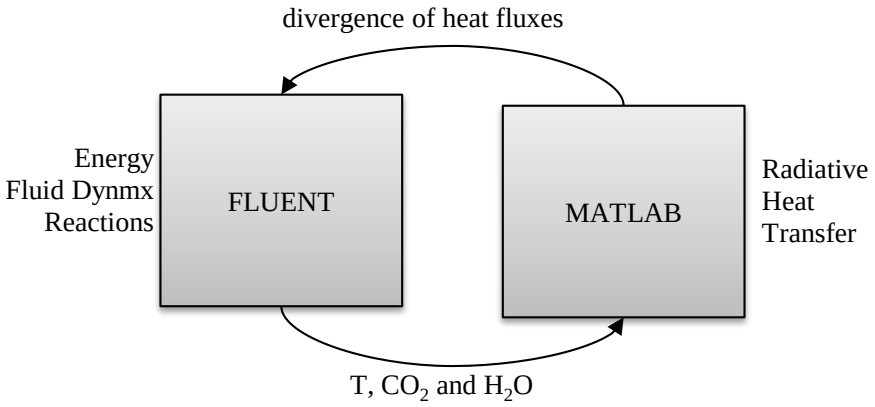

Figure 3.1: The computational model schematic.

characteristics are given in detail in Section Flame Model.

Solving flow equations will yield temperature and molar concentrations profiles, which are used to find radiative intensity by using radiation solver. The radiatively participating gases after combustion are carbon dioxide and water vapor, while soot radiation is ignored. Their spectral effects are modeled by statistical narrow band correlated-k. Discrete ordinates method is used to solve radiative transfer equation.

3.1. Governing Equations

All equations are given in Cartesian geometry at steady state. The flow is considered as turbulent and k-ε model is used. Velocity term in Navier-Stokes equations is represented by using Reynolds averaging, which is decomposed into mean and fluctuating components. The velocity is then represented as,

$$u_i = \bar{u}_i + u_i' \tag{3.1}$$

where $\bar{u}_i$ and u_i' are mean and fluctuating velocity components (i=1,2). The other scalar quantities such as pressure, energy, and species concentration are also represented by using Reynolds averaging, such as

$$\phi = \bar{\phi} + \phi' \tag{3.2}$$

3.1.1. Continuity Equation

$$\frac{\partial}{\partial x_i}(\rho u_i) = 0 \tag{3.3}$$

3.1.2. Momentum Equations

$$\frac{\partial}{\partial x_j}(\rho u_i u_j) = -\frac{\partial p}{\partial x_i} + \frac{\partial}{\partial x_j}\left[\mu\left(\frac{\partial u_i}{\partial x_j} + \frac{\partial u_j}{\partial x_i} - \frac{2}{3}\delta_{ij}\frac{\partial u_l}{\partial x_l}\right)\right] + \frac{\partial}{\partial x_j}(-\rho\overline{u_i' u_j'}) \tag{3.4}$$

3.1.3. Heat Equation

$$\frac{\partial}{\partial x_i}[u_i(\rho E + p)] = \frac{\partial}{\partial x_j}\left[k_{eff}\frac{\partial T}{\partial x_j} + u_i\left(\mu_{eff}\left(\frac{\partial u_j}{\partial x_i} + \frac{\partial u_i}{\partial x_j} - \frac{2}{3}\mu_{eff}\frac{\partial u_k}{\partial x_k}\delta_{ij}\right)\right)\right] + S_h \tag{3.5}$$

where E is total energy, which is defined as

$$E = h - \frac{p}{\rho} + \frac{v^2}{2}$$

where h is sensible enthalpy for ideal gas as

$$h = \sum_j Y_j h_j$$

where Y_j is the mass fraction of species j and

$$h_j = \int_{T_{ref}}^{T} c_{p,j} dT \tag{3.6}$$

k_{eff} is the effective thermal conductivity, which is defined for realizable k-ε turbulence model as,

$$k_{eff} = k + \frac{c_p \mu_t}{Pr_t} \tag{3.7}$$

where k, in this case, is the thermal conductivity, Pr_t is turbulent Prandtl number, which is taken as constant value of 0.85. μ_t is turbulent viscosity, which is calculated by using k-ε parameters as

$$\mu_t = \rho C_\mu \frac{k^2}{\varepsilon} \tag{3.8}$$

C_μ is calculated as

$$C_\mu = \frac{1}{A_0 + A_s \frac{kU*}{\varepsilon}} \tag{3.9}$$

Model constants A_0 and A_s are given 4.04 and $\sqrt{6}cos\phi$ respectively, where

$$\phi = \frac{1}{3}\cos^{-1}(\sqrt{6}W),\ W = \frac{S_{ij}S_{jk}S_{ki}}{\tilde{S}^3},\ \tilde{S} = \sqrt{S_{ij}S_{ij}},\ S_{ij} = \frac{1}{2}\left(\frac{\partial u_j}{\partial x_i} + \frac{\partial u_i}{\partial x_j}\right)$$

$$U^* \equiv \sqrt{S_{ij}S_ij + \tilde{\Omega}_{ij}\tilde{\Omega}_{ij}}$$

and

$$\tilde{\Omega}_{ij} = \Omega_{ij} - 2\varepsilon_{ijk}\omega_k$$

$$\Omega_{ij} = \overline{\Omega_{ij}} - \varepsilon_{ijk}\omega_k$$

$\overline{\Omega_{ij}}$ is the mean rate-of-rotation tensor viewed in a moving reference frame with the angular velocity ω_k. S_h is defined as a source function, which includes heat addition due to radiative transfer, which equals to the divergence of radiative heat flux (Equation 2.53), and due to chemical reaction, such as

$$S_h = S_{h,rdn} + S_{h,rxn} \tag{3.10}$$

where $S_{h,rxn}$ is

$$S_{h,rxh} = -\sum_j \frac{h_j^0}{M_j}\mathcal{R}_j \tag{3.11}$$

where h_j^0 is the enthalpy of formation of species j and $\mathcal{R}_j$ is the volumetric rate of creation of species j. The modeled realizable k-ε turbulent transport equations are given as follows.

3.1.4. Transport Equations for the Realizable k-ε Model

$$\frac{\partial}{\partial x_j}(\rho k u_j) = \frac{\partial}{\partial x_j}\left[\left(\mu + \frac{\mu_t}{\sigma_k}\right)\frac{\partial k}{\partial x_j}\right] + G_k + G_b - \rho\varepsilon - Y_M \tag{3.12}$$

$$\frac{\partial}{\partial x_j}(\rho \varepsilon u_j) = \frac{\partial}{\partial x_j}\left[\left(\mu + \frac{\mu_t}{\sigma_\varepsilon}\right)\frac{\partial \varepsilon}{\partial x_j}\right] + \rho C_1 S\varepsilon - \rho C_2 \frac{\varepsilon^2}{k + \sqrt{\nu\varepsilon}} + C_{1\varepsilon}\frac{\varepsilon}{k}C_{3\varepsilon}G_b \tag{3.13}$$

where

$$C_1 = max(0.43, \frac{\eta}{\eta + 5}),\ \eta = S\frac{k}{\varepsilon},\ \text{and}\ S = \sqrt{2S_{ij}S_{ij}}$$

Model constants $C_{1\varepsilon}$, C_2, σ_k, and σ_ε are given as 1.44, 1.9, 1.0, and 1.2 respectively. Another model parameter is given as $C_{3\varepsilon} = \tanh(|v/u|)$, where v is the component of the flow velocity parallel to the gravitational vector. G_k, G_b, and Y_M are called as generation of turbulence kinetic energy due to the mean velocity gradients, due to buoyancy, and contribution of the fluctuating dilatation in compressible turbulence to the overall dissipation rate. They are defined for ideal gas as

$$G_k = -\rho\overline{u_i' u_j'}\frac{\partial u_j}{\partial x_i}$$

$$G_b = -g_i \frac{\mu_t}{\rho Pr} \frac{\partial \rho}{\partial x_i}$$

$$Y_M = 2\rho\varepsilon \frac{k}{\gamma RT}$$

where g_i is the component of the gravitational vector in the ith direction.

3.1.5. Species Transport Equations

Species transport and finite-rate chemistry equations about volumetric reactions are given in equation 3.14.

$$\nabla \cdot (\rho \vec{\nabla} Y_i) = -\nabla \cdot \vec{J_i} + R_i \tag{3.14}$$

where Y_i is the local mass fraction of each species, R_i is the net rate of production of species i by the chemical reaction, which is given in Equation 3.15, $\vec{J_i}$ is mass diffusion in turbulent flows, which is given in Equation 3.16.

$$R_{i,r} = \nu'_{i,r} M_{w,i} A \rho \frac{\varepsilon}{k} min_{\mathcal{R}} \left(\frac{Y_{\mathcal{R}}}{\nu'_{\mathcal{R},r} M_{w,\mathcal{R}}} \right) \tag{3.15}$$

$$R_{i,r} = \nu'_{i,r} M_{w,i} A B \rho \frac{\varepsilon}{k} \frac{\sum_P Y_P}{\sum_j^N \nu''_{j,r} M_{w,j}}$$

where Y_P is the mass fraction of any product species, P, $Y_{\mathcal{R}}$ is the mass fraction of a particular reactant, $\mathcal{R}$, and A and B are empirical constants equal to 4.0 and 0.5, respectively.

$$\vec{J_i} = -\left(\rho D_{i,m} + \frac{\mu_t}{Sc_t} \right) \nabla Y_i - D_{T,i} \frac{\nabla T}{T} \tag{3.16}$$

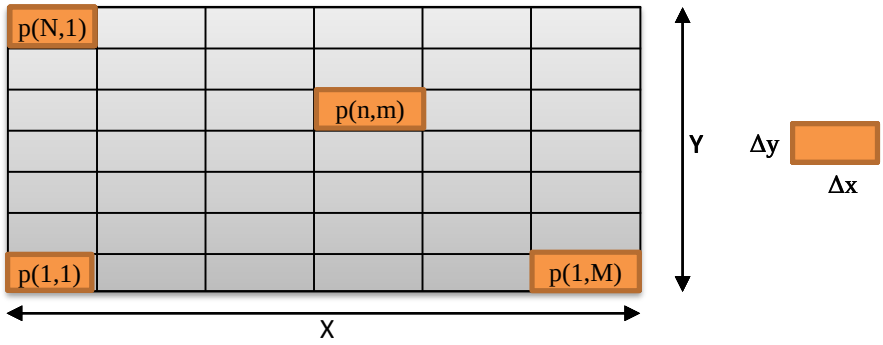

Figure 3.2: Geometry and mesh.

where Sc_t is the turbulent Schmidt number, which is taken as 0.7. $D_{i,m}$ is the mass diffusion coefficient, $D_{T,i}$ is the thermal diffusion coefficient.

3.2. Geometry and Mesh

The enclosure and medium is described numerically by dividing two dimensional space into uniform N-by-M rectangular mesh given in Figure 3.2. X and Y define the rectangular size while N and M are the number of elements in each side respectively. Δx and Δy are cell dimensions in x and y direction. Each cell has five points that is previously described in Figure 2.9; One is at the center of the cell, the others are at the middle of four edges, namely north, south, east and west. Exactly same mesh is generated both on radiation solver and flow solver.

3.3. Model Description

Developed model is aimed to solve non-gray radiative transfer of a flame and its automated coupling with the flow solver. Non-gray radiative calculations are done along non-homogeneous paths of temperature and molar concentrations considering spectral effects. When we look from engineering point of view, heat flux and its divergence are the most meaningful physical values needed to be found while modeling the radiative transfer. In that manner, a flame's spectral heat flux at any point of interest on the wall and its spectral divergence of radiative flux at any arbitrary point within the flame are calculated with line-by-line accuracy. This accuracy can also be achieved using line

data from high temperature database such as HITEMP; however only for H_2O there are over 5 million lines defined in this database. Calculations can only be done with the most powerful processors which is not practical enough for an engineering application.

Most of development time is spent on radiation solver to integrate k-distributions in order to decrease computational time significantly. Automation of flow solver on radiation solver is later established. Basic flowchart of this automation process is given in Figure 3.3.

To start from beginning, 1.0 by 0.5 m rectangular fluid enclosed by black walls at 300 K with meshing sizes 20 by 20 is modeled that is illustrated in Figure 3.2. A sample flame model is described on flow solver giving specific geometry and mesh sizes and defining boundary conditions. It is a steady combustion of methane creating high temperature participating gases of CO_2 and H_2O. Details can be found in Section Flame Model. Same configuration of geometry and mesh sizes are also described on radiation solver. This procedure is the initial inputs for the model, radiation and flow solvers are communicated from MATLAB environment using cfd software's text user interface (TUI) over MS-DOS commands.

User defined functions (udf) on cfd software allow you to define properties or subroutines that are not configurable with the sofware graphical interface, but a code is written for them. In this work, two user defined functions (see appendix) are employed in order to input calculated divergence of heat flux field on flow solver. In the first one, called "matlab-to-fluent", reads the text file "dohf.txt" containing divergence of heat flux for every point on the mesh. Then second one called "energy" set these values as radiative source function in energy equation. After writing these piece of codes, they are saved as C-file, and are hooked to flow solver as "interpreted udf' such a way that under define menu, user-defined and then interpreted-functions are selected. Instructive information about hooking interpreted-functions is in the appendix. Then, under menu define, user-defined and function hooks, the interpreted functions are hooked as "adjust" and "source" functions correspondingly. Software is ready to solve given case under this setup. Iterations will continue until sufficient convergence criteria (default

setting) is reached. The fields of temperature and molar fractions of CO_2 and H_2O are three important results from the solution. These results are written in a text file named "thc.txt" using TUI command, which is given as appendix in Section Main Code. Next, radiation solver takes these three fields as input while calculating divergence of heat flux. The details of radiation solver is given in Section Radiation Solver. Once the solution is converged, radiation model is activated in the flow solver for only one more iteration in order to calculate absorption coefficients using Equation 3.21 for corresponding temperature and molar concentration field using method of weighted sum of gray gases. They are total value of absorption for whole spectrum which are written in a text file named "abs.txt". The TUI command for absorption coefficient is similar to temperature field, expect "absorption coefficient" rather than "temperature" should be coded into TUI. These absorption coefficients later are used in radiation solver in order to get gray solution.

Number of iterations done (NoI) is also returned from cfd solver which is the convergence mechanism between radiation and cfd calculations. If NoI is greater than two, rte solver will always calculate a new divergence. If it is smaller, it can be said that the solution is converged, because the given new divergence term does not effect anything on cfd solver.

3.4. Flame Model

The description of the flame used in the current model is given in Figure 3.4. There is main air inlet on the left and also there are two small air inlets on the bottom wall at two sides of fuel inlet in order to control flame shape. There is pressure outlet on the right. All walls are treated as black and also at a constant temperature at value of 300K. The reaction of combustion of CH_4 is only considered which is

$$CH_4 + 2O_2 \rightarrow CO_2 + 2H_2O \tag{3.17}$$

Air is assumed as consisting of 23% of O_2 and 77% of N_2 on molar basis. The velocity of air is taken as 0.5 m/s while fuel 10 m/s. 10% turbulent intensity for both air and

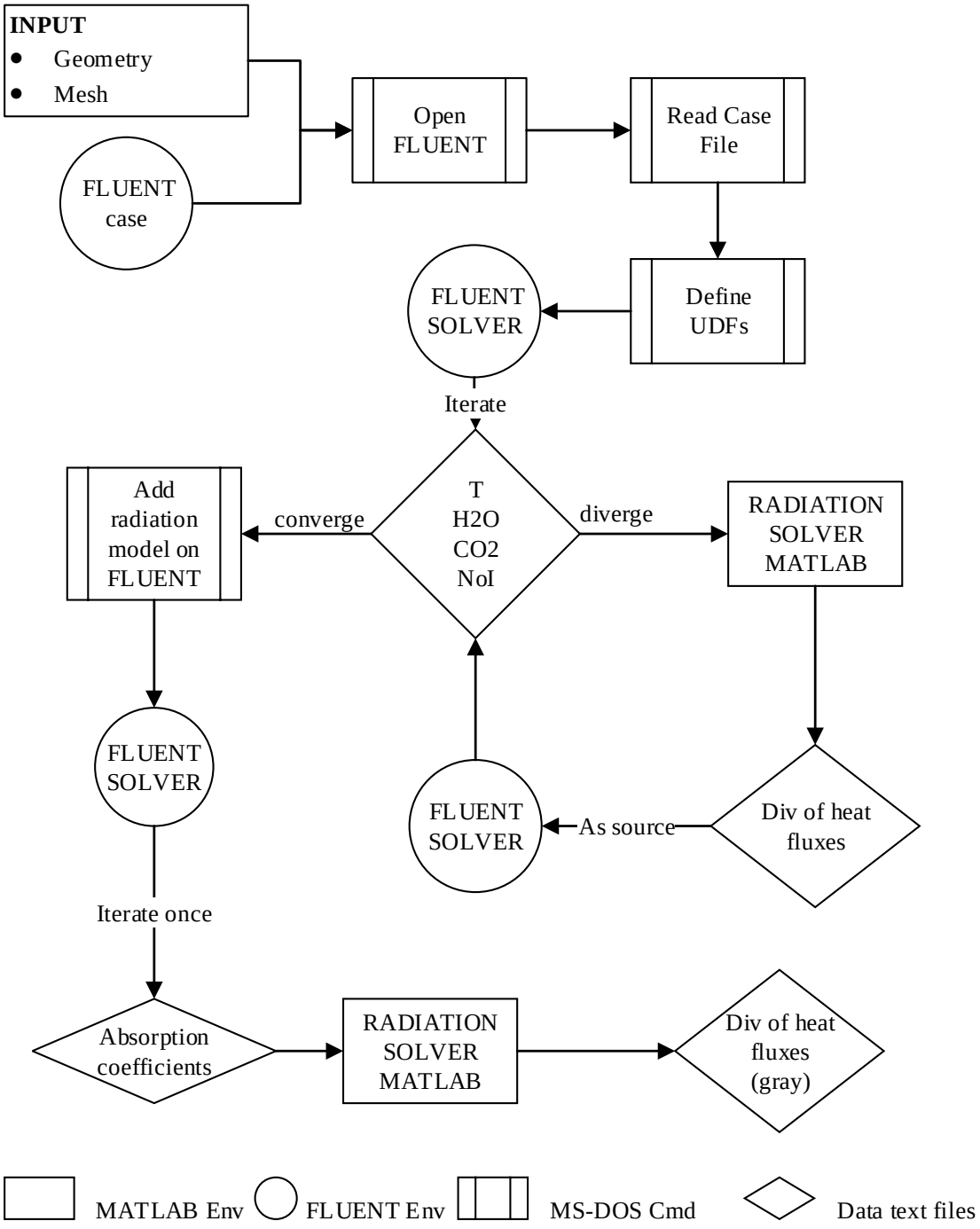

Figure 3.3: Flow chart of current model.

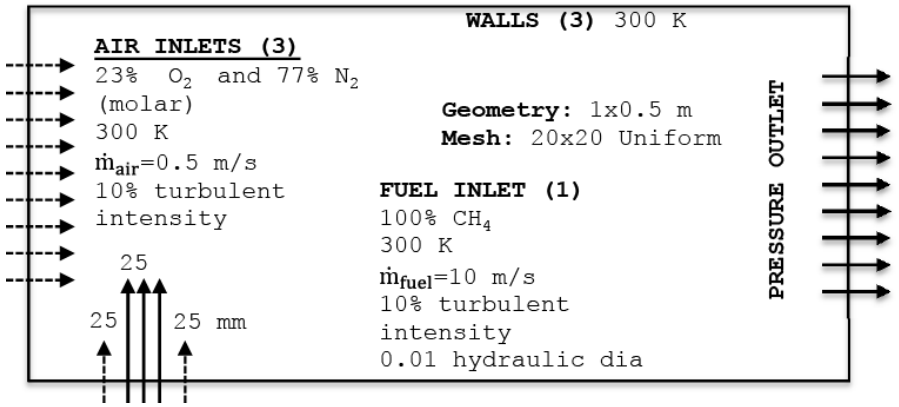

Figure 3.4: Flame model configuration details.

fuel inlets, 0.01 and 0.44 hydraulic diameter correspondingly used during calculations. When flow solver is not coupled with radiation model, flow solver employs WSGG model in order to model gray gas radiation. The description of WSGG used during non-coupled gray radiation calculations is given next.

3.4.1. Gray absorption coefficient calculation in flow solver

Weighted sum of gray gas model takes into account the total emissivity over the distance s can be given as,

$$\epsilon = \sum_{j=0}^{N} a_{\epsilon,j}(T)(1 - \exp(-\kappa_j ps)) \tag{3.18}$$

where $a_{\epsilon,j}$ is the emissivity weighting factor for the jth fictitious gray gas. $a_{\epsilon,j}$ and κ_j values are taken from references [21, 31]. Temperature dependence of Equation 3.18 is given as [21, 31, 32]

$$a_{\epsilon,j}(T) = \sum_{i=1}^{I} b_{\epsilon,j,i} T^{i-1} \tag{3.19}$$

Because the coefficients $b_{\epsilon,j,i}$ and κ_j are not changing so fast with ps and T, they can be assumed constant for a wide range of these parameters. The corresponding coefficients for CO_2 and H_2O at various partial pressures are given in [21]. The values can be used for $0.001 < ps < 10.0$ atm-m and $600 < T < 2400$ K. If $\kappa_j ps << 1$, Equation 3.18

reduces to

$$\epsilon = \sum_{j=0}^{N} a_{\epsilon,j} \kappa_j p s \tag{3.20}$$

Absorption coefficient k, is calculated for a single gray gas in flow solver such a way

$$k = \sum_{j}^{J} a_{\epsilon,j} \kappa_j p \tag{3.21}$$

which does not depend on s. Mostly, k is approximated as

$$k = -\frac{\ln(1-\epsilon)}{s} \tag{3.22}$$

4. RESULTS

Current model gives spectral and total divergence of heat flux of a combustion environment. In order to show that, spectral and total calculations of a sample combustion case are done using a commerical cfd solver which is explained in detail in Flame Model section. Total and spectral divergence of heat flux and total and spectral wall heat flux are calculated and they are given in Non-gray Results section. Later, for the same configuration, absorption coefficients are calculated by using weighted-sum-of-gray-gas model for a single gray gas, then they are used in current model to find divergence of heat flux and wall heat flux for a gray case. These values are used to compare non-gray solution. These results are presented in Section Comparison with Gray Solution".

The sample flame is solved by coupling flow and radiation solvers. The details of the case is given in Figure 3.4. Next, resulting temperature, molar concentration and absorption coefficient fields are presented. Temperature field can be seen in Figure 4.1, which has the highest temperature level of 1000K, while 400 K is recorded as low temperature level. Molar fractions are 0.00 - 0.17 and 0.00 - 0.8 for H_2O and CO_2 correspondingly. The contour plots of molar fraction of H_2O and CO_2 are given in Figures 4.2 and 4.3. Absorption coefficients are exported directly from flow solver, which utilizes weighted-sum-of-gray gases assumption. The details are given in Section 3.4.1. The absorption coefficient ranges between 0.05 - 4.19 m^{-1}. Absorption coefficient inside medium is illustrated in Figure 4.4.

4.1. Non-gray Results

Three results are presented in this section, namely spectral divergence of heat flux at specific points within medium (Figure 4.5), contour plot of total divergence of heat flux (Figure 4.6) and spectral incoming and outgoing wall heat flux (Figure 4.7).

Spectral radiative source terms are given in Figure 4.5, two points are selected

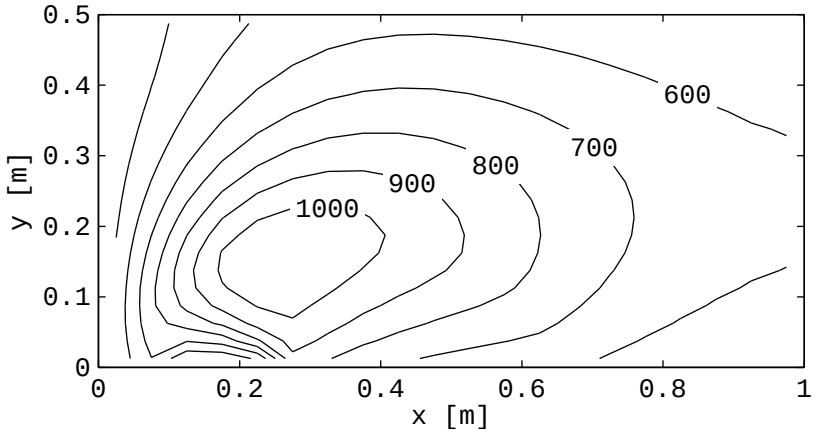

Figure 4.1: Temperature distribution of the solution from radiative solver coupling, [K].

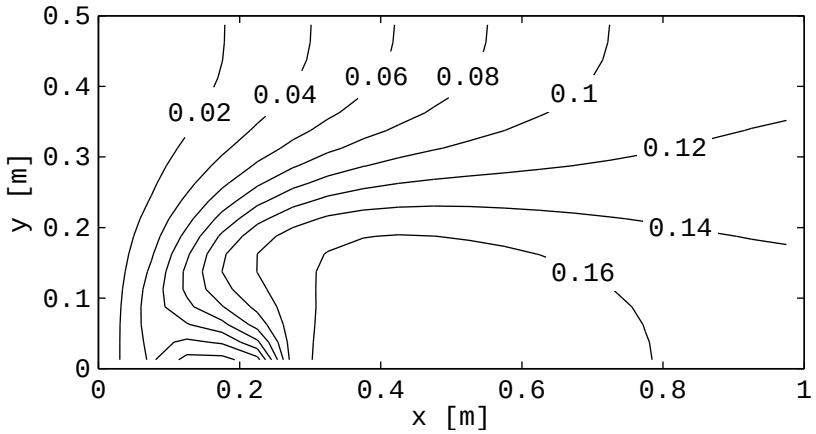

Figure 4.2: H_2O distribution of the solution from radiative solver coupling, [% molar].

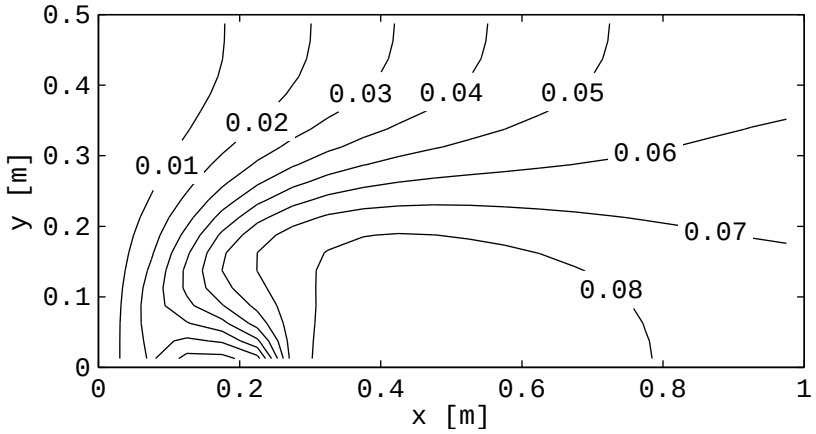

Figure 4.3: CO_2 distribution of the solution from radiative solver coupling, [% molar].

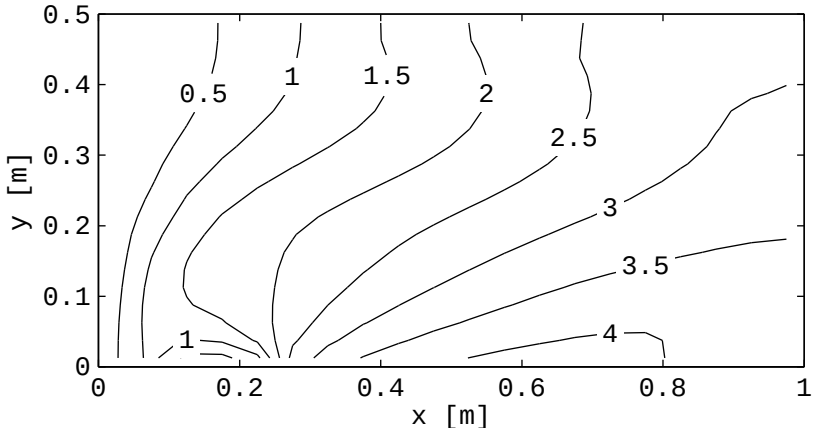

Figure 4.4: Absorption coefficient calculated on non-coupled flow solver for given temperature, molar concentrations, [m^{-1}].

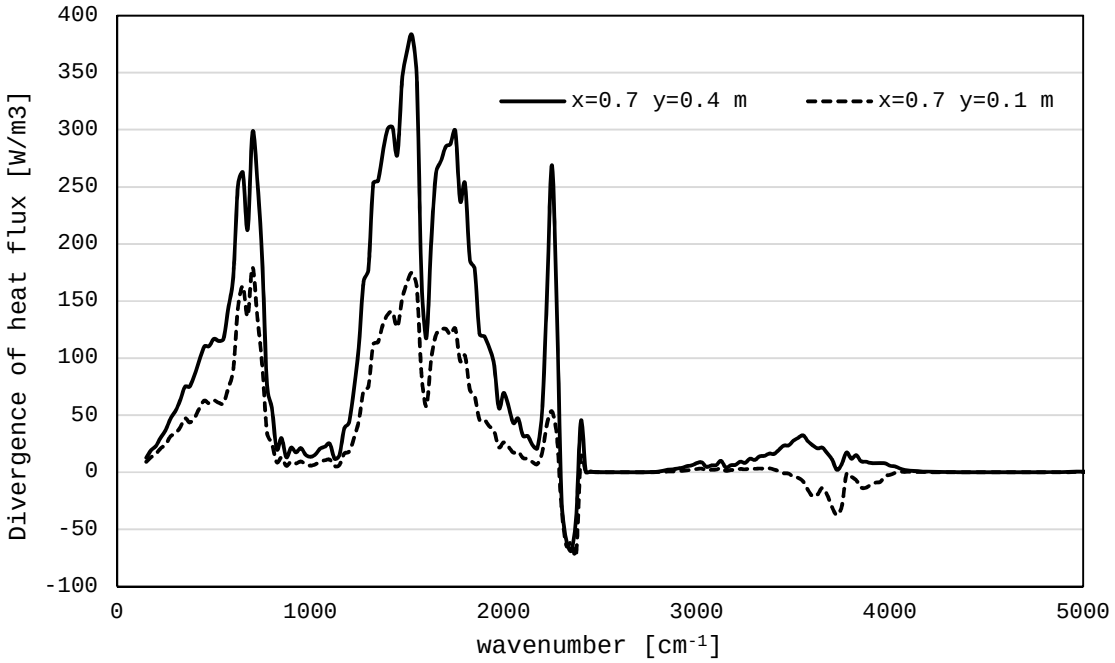

Figure 4.5: Divergence of heat flux against wave number at two locations (x=0.7 y=0.4 and x=0.7 y=0.1 m).

in the medium which are located at (0.7, 0.4 m) and (0.7, 0.1 m). Divergence of heat flux across the spectrum is calculated between from wave numbers 150 to 9300 cm^{-1}; however, wave numbers between 150 and 5000 cm^{-1} is presented in the figure due to zero divergence at higher wave numbers. In Figure 4.6, total divergence of heat flux for entire medium is plotted in a contour plot. If temperature field in Figure 4.1 is compared with this figure, they are similar. Higher temperature zones generate greater amount of energy as expected. Using this figure, the exact amount of energy addition -positive values- or energy loses -negative ones- can be seen. The area rounded with "80 line" is the core of the flame, while negative lines are near air inlet creating colder areas. Maximum divergence of heat flux is calculated higher than 80 kW/m^3, minimum divergence is recorded as -5 kW/m^3. Spectral wall heat flux is presented in Figure 4.7, which may be the most meaningful from engineering point of view.

While estimating wall temperatures, incoming and outgoing heat flux are important. Thermal radiative outgoing and incoming wall heat flux at north wall are plotted against wave number in Figure 4.7. Dashed line is blackbody emission at constant temperature. It has maximum at 500 cm^{-1} band with an order of 5 W/m^2. Incident

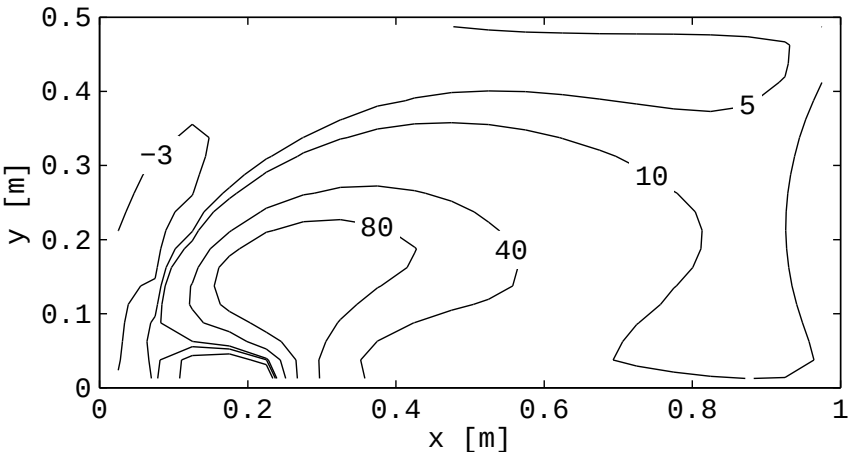

Figure 4.6: Contour plot of heat flux divergence in kW/m^3.

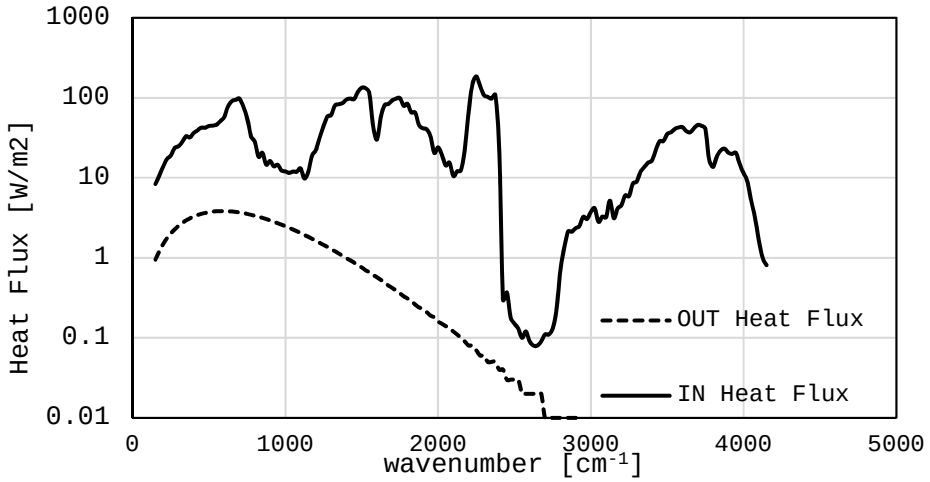

Figure 4.7: Incoming spectral wall heat flux and outgoing spectral wall heat flux against wave number at the middle point of north wall.

radiation shows higher trend which means that net heat flux is going into the wall. The calculation is done for all bands between 150-9300 cm^{-1}, but values smaller than 0.01 W/m^2 are omitted, and not shown on the figure.

4.2. Comparison with Gray Solution

In this part, non-gray solution is compared with gray results. The gray calculations are done with the temperature and gas composition given in Figure 4.1, 4.2 and 4.3. The gray absorption coefficient is taken as in Figure 4.4. In the first two figures,

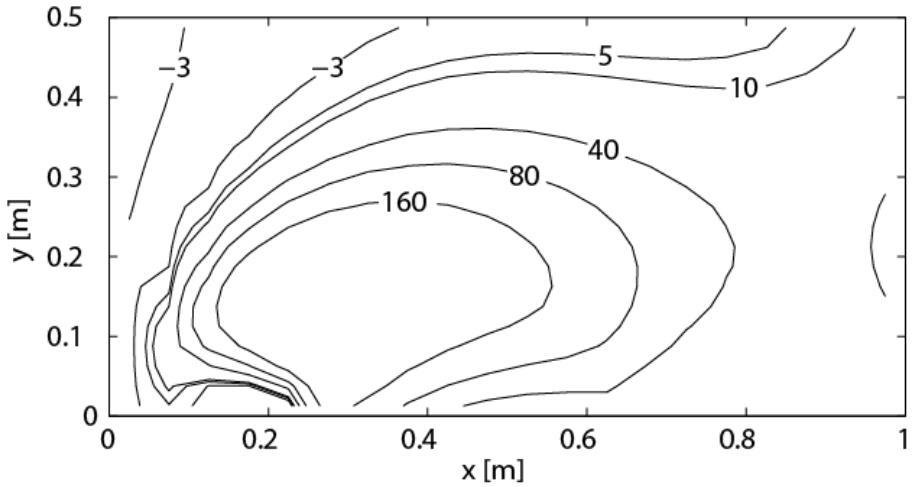

Figure 4.8: Divergence of heat flux of gray case in kW/m^3. Comparison with non-gray case in Figure 4.6 can be made.

divergence of heat flux (Figure 4.8) and incoming wall heat flux to the walls located at north and east (Figure 4.9) are presented.

First, divergence of heat flux is plotted in Figure 4.8. Curves seem to follow same trend in terms of local maximum and minimums; but gray case shows higher divergence. Divergence of heat flux of 160 kW/m^3 line is plotted for gray case which is way above for non-gray case 80 kW/m^3.

Non-gray incoming heat flux at east and north walls are compared with gray solution in Figure 4.9. The lines without markers represent incident radiations on the north wall, with marker lines are for east wall radiative heat flux. Gray solution gives higher heat flux than non-gray solution. The maximum incoming heat flux at north wall in non-gray solution is calculated as 8 kW/m^2 at 0.25 m which is 25 kW/m^2 in gray solution at the same point. Similar comparison for east wall is also made and is presented on the same plot. On the east wall incident radiation is lower than north side which is expected, because the flame is closer to north wall and also east wall is the exit for leaving gases. Same calculations are done for other two walls, but they are not provided to prevent excessive information. Outgoing heat flux due to blackbody emission is calculated as a constant value of 140 W/m^2 for both cases.

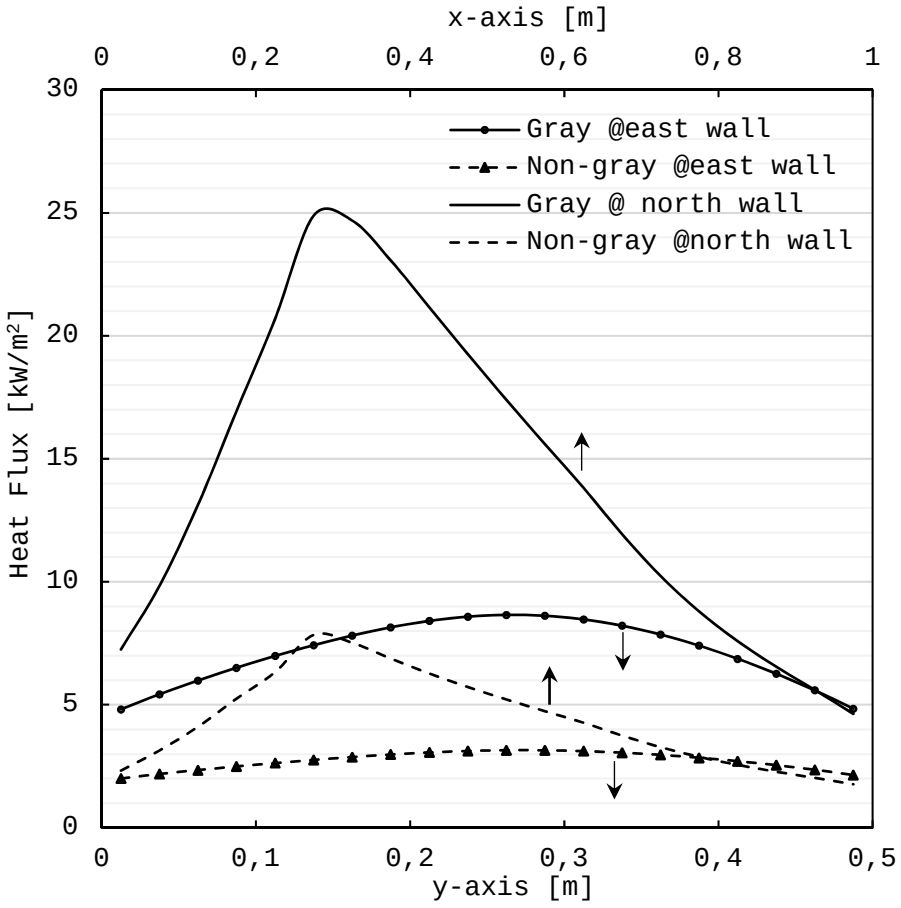

Figure 4.9: Incident wall heat flux comparing gray and non-gray cases at east and north walls.

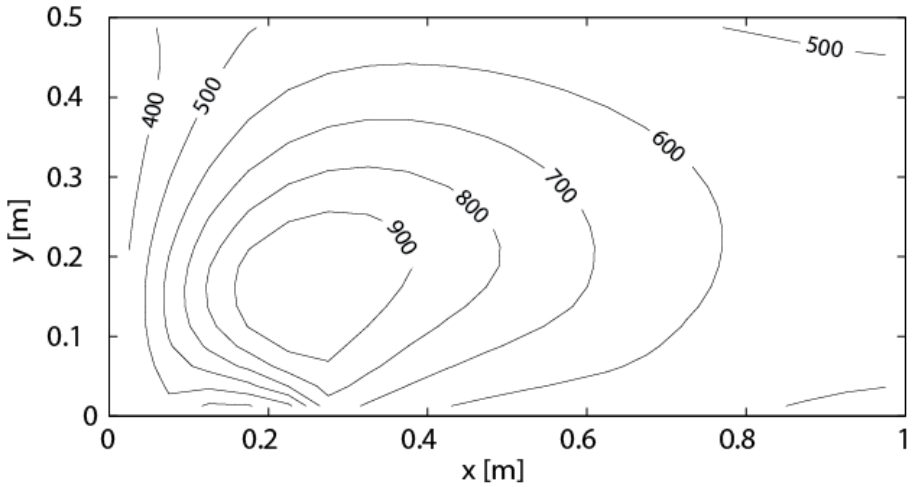

Figure 4.10: Temperature distribution of gray case solution [K]. Comparison can be made with temperature distribution of non-gray case in Figure 4.1.

The resulting temperature field of gray-gas model coupled with flow equations is given in Figure 4.10. When non-gray solution in Figure 4.1 is compared with this figure, considerable changes can be observed. Taking into account spectral effects leads to smaller radiative source term which then yields greater temperature values. Gray model, on the other hand, approximates higher radiative source terms.

5. CONCLUSION

In the first part of the study, two dimensional radiative heat transfer problem of non-gray gas profiles of temperature and molar concentrations is numerically solved by using statistical narrow band correlated-k model. The main motivation is that the solution is line-by-line accurate and also it has spectral results. During modeling of radiating gases, discrete ordinates method is used in order to discretize radiative transfer equation. The participating medium is assumed as it is enclosed with black walls and divided into equal rectangular control volumes. Later, the radiative transfer equation is solved in every control volumes, ordinates and narrow bands in order to obtain radiative intensities. Spectral and total wall heat fluxes are calculated from these intensities. The radiative source term in energy equation which is divergence of heat flux is also calculated. The radiative model is tested and validated by comparing line-by-line benchmark results.

In the second part of the study, radiative solver is coupled with cfd solver considering the equations of fluid dynamics, energy, reaction and species transport. A flame model is used on flow solver in order to show a sample calculation which is basically the turbulent combustion of CH_4 in a rectangular two dimensional enclosure. The radiative source terms are calculated by using radiative solver which takes the data of temperature and molar concentration profiles obtained from the flow solver as output. The coupling of solvers is established by using cfd software's text user interface over MSDOS command window. Then, source terms are added to energy equation on flow solver. A convergence mechanism between two systems is set. Finally, the resulting total and spectral wall heat fluxes are computed and compared with gray case solution.

The results are presented in two sections which are non-gray and gray results. In the first section, the profile of spectral divergence of heat flux is plotted at two locations inside medium. Contour graph of total divergence of heat flux field is plotted in order to visualize overall energy additions and losses. The outgoing and incoming spectral wall heat fluxes are also plotted.

In the second part of results, gray solution is compared with non-gray one in terms of total divergence and wall heat fluxes. The results are plotted for incident and leaving intensities on south and north walls. Finally, gray solution is provided with coupling to flow equations. Temperature field of coupled gray solution is compared with coupled non-gray one in the very last figure. The comparison shows that the temperature is underestimated for the gray case.

As for future work, the numerical model of radiative heat transfer using statistical narrow band may be expanded in further studies to cover three dimensional media, to satisfy scattering effects and to include more participating molecular gases apart from carbon dioxide and water vapor.

APPENDIX A: Validation Cases

A.1. Case Zero

In case zero, discrete ordinates method is tested with a constant absorption coefficient κ_η=0.5 in a homogeneous medium at 1000 K. The results looks accurate when it is compared with previous work of Chu *et al.* [29]. The solutions labeled as *DOM* and *Ray Tracing* in their study having a very good agreement with *2drte* that can be seen in Figure A.1.

A.2. Case One

In case one, the medium is at constant temperature of 1000 K and containing only CO_2 at molar concentration of 0.1. The results are presented in Figure A.2. Only one $k(g)$ is calculated for this case because all points inside medium having constant temperature and molar fraction. Thus, it is a perfect case to test correct contribution of all 96 CO_2 bands.

A.3. Case Two

In case two, CO_2 is the only participating gas having non-homogeneous paths of temperature and mole fraction. This case is well suited to test k-distributions of CO_2 under varying temperatures. Contour plot of the mole fraction of CO_2 inside medium is plotted in Figure A.3. Temperature contour is given previously in Figure 2.15. Divergence of heat flux is plotted in Figure A.4 along in x and y direction at y=0.25 and x=0.5 correspondingly.

A.4. Case Three

In case three, the medium is at constant temperature of 1000 K and containing only H_2O at molar concentration of 0.2. The results are presented in Figure A.5. Only

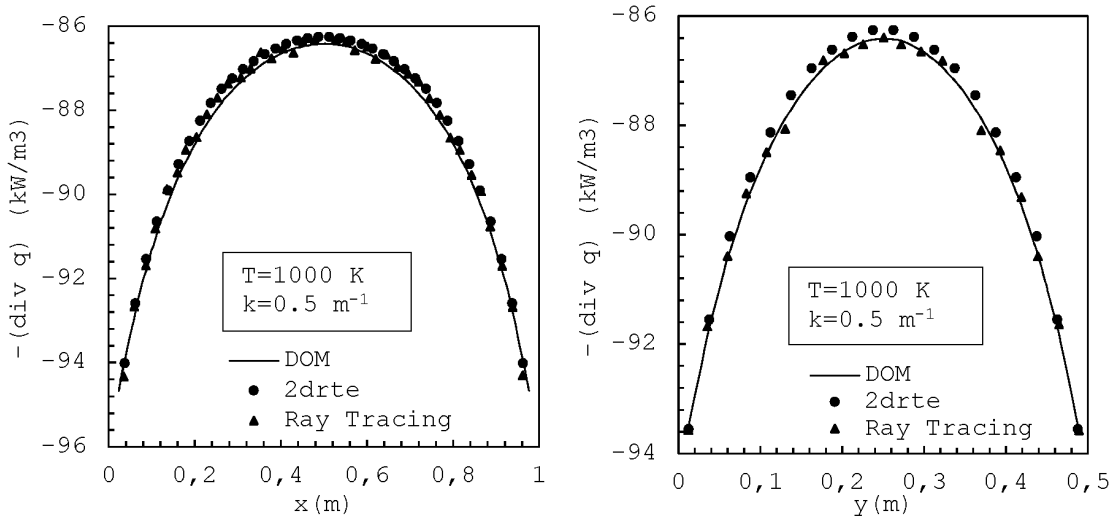

Figure A.1: Case Zero: Distribution of radiative source term along $y = 0.25$ (left) and $x = 0.50$ (right) in kW/m^3 [9].

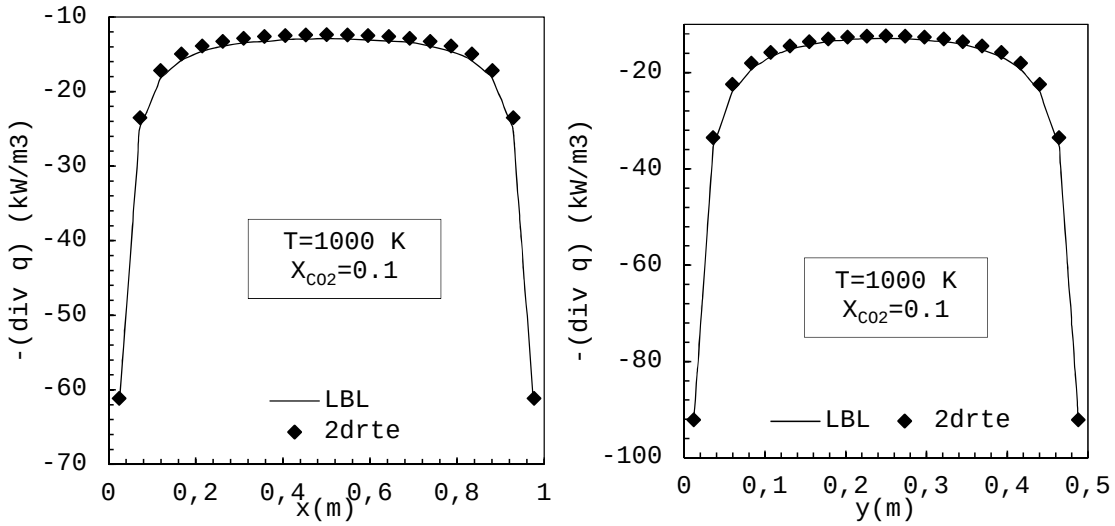

Figure A.2: Case 1:Distribution of radiative source term along $y = 0.25$ (left) and $x = 0.50$ (right) in kW/m^3 [9].

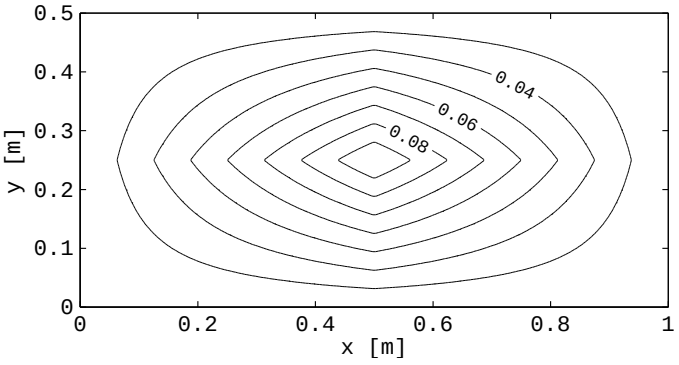

Figure A.3: Molar concentration profile of carbon dioxide for case two.

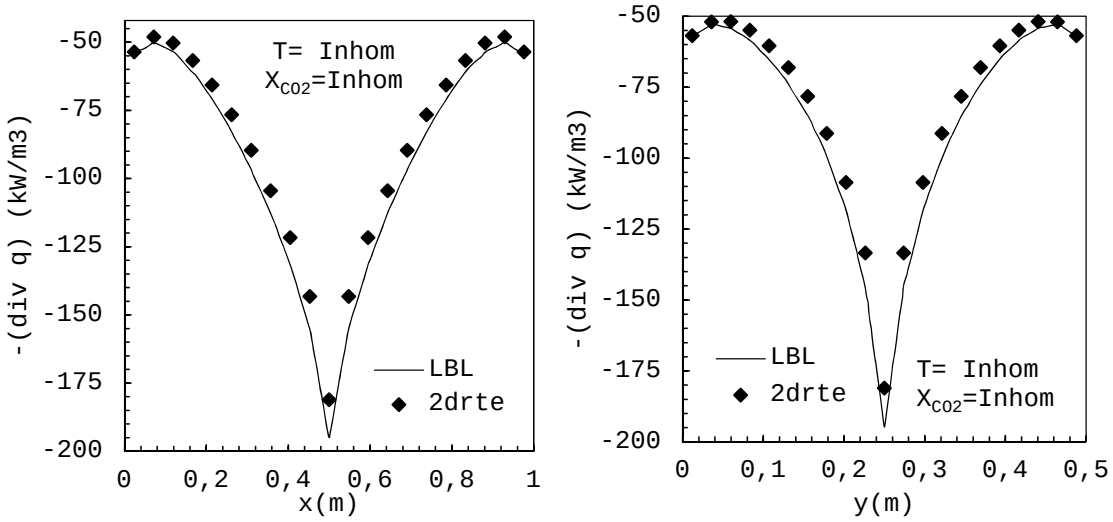

Figure A.4: Case Two: Distribution of radiative source term along $y = 0.25$ (left) and $x = 0.50$ (right) in kW/m^3 [9].

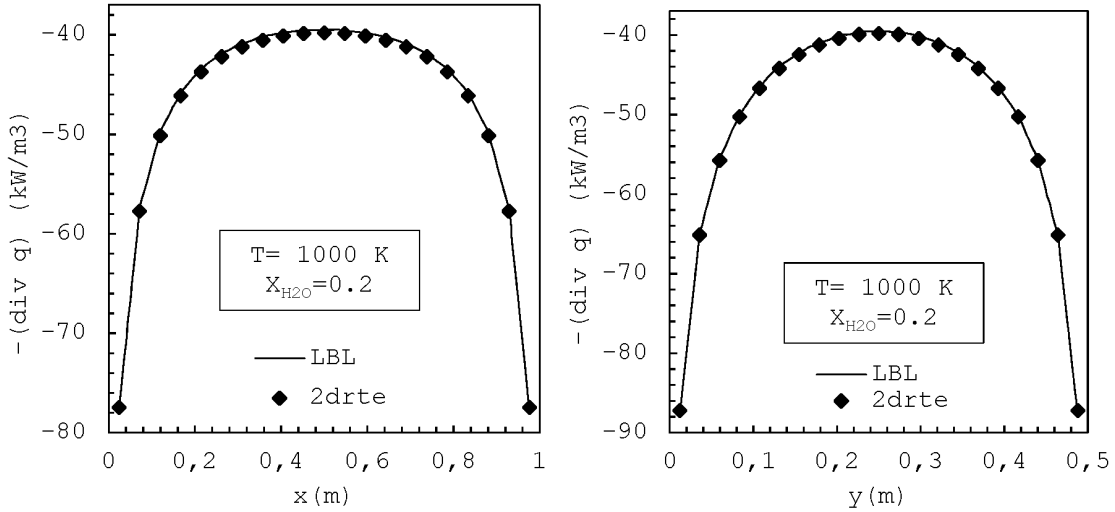

Figure A.5: Case Three: Distribution of radiative source term along $y = 0.25$ (left) and $x = 0.50$ (right) in kW/m^3 [9].

one $k(g)$ is calculated for this case because all points inside medium having constant temperature and molar fraction. Thus, it is a perfect case to test correct contribution of all 367 H_2O bands.

A.5. Case Four

In case four, H_2O is the only participating gas having non-homogeneous paths of temperature and mole fraction. This case is well suited to test k-distributions of H_2O under varying temperatures. Contour plot of the mole fraction of H_2O inside medium is plotted in Figure A.6. Temperature contour is given previously in Figure 2.15. Divergence of heat flux is plotted in Figure A.7 along in x and y direction at y=0.25 and x=0.5 m correspondingly.

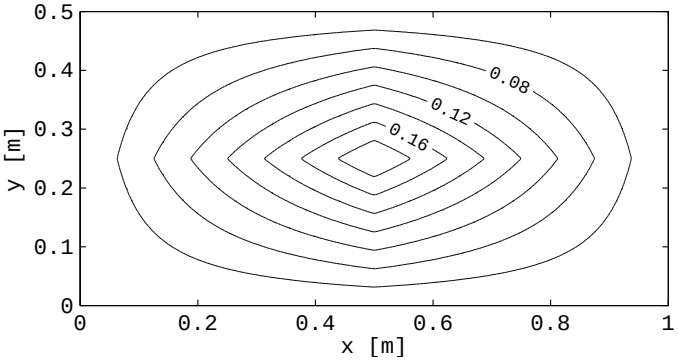

Figure A.6: Molar concentration profile of water vapor for case four.

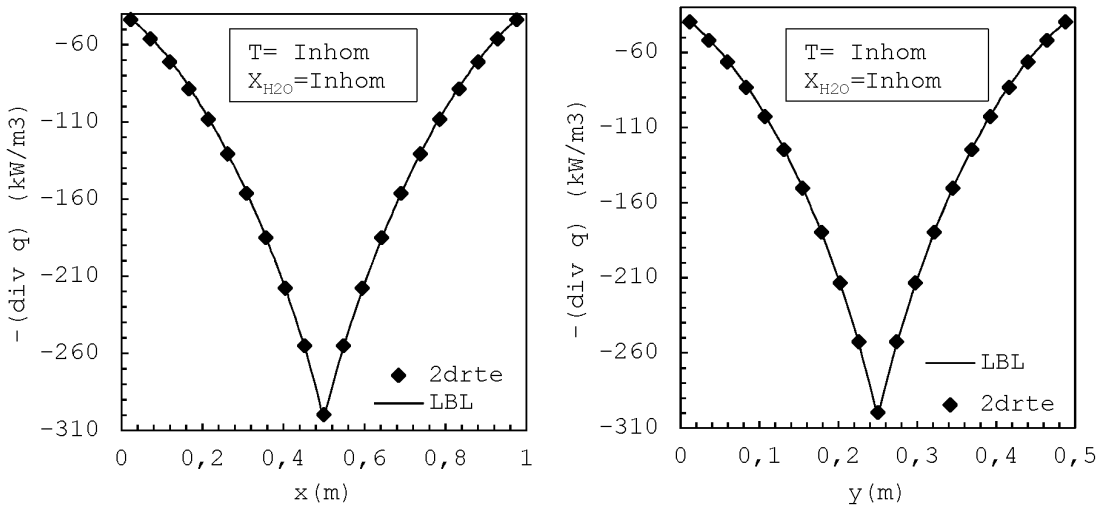

Figure A.7: Case Four:Distribution of radiative source term along $y = 0.25$ (left) and $x = 0.50$ (right) in kW/m^3 [9].

APPENDIX B: T7 Quadrature Set

Table B.1: T_7 Quadrature Set.

i	ξ_i	η_i	W_i
1	0.997241374054808	0.052486388108147	0.0273981172069195
2	0.968364052270084	0.060522753266880	0.0419359596096118
3	0.968364052270084	0.242091013067521	0.0419359596096056
4	0.986440050415621	0.116051770637132	0.0370139280413859
5	0.878458591919332	0.0675737378399486	0.0582067125108141
6	0.916949300616178	0.282138246343439	0.0660565456086317
7	0.878458591919332	0.473016164879640	0.0582067125108132
8	0.933333333333333	0.133333333333333	0.0559374747989008
9	0.933333333333333	0.333333333333333	0.0559374747989008
10	0.705345615858598	0.0705345615858598	0.0660962551843145
11	0.778498944161523	0.311399577664609	0.0882964747628847
12	0.778498944161523	0.544949260913066	0.0882964747628838
13	0.705345615858598	0.705345615858598	0.0660962551843145
14	0.800132264198639	0.145478593490662	0.0723426374612526
15	0.841191024192060	0.382359556450936	0.0838150329949681
16	0.800132264198639	0.581914373962646	0.0723426374612526
17	0.473016164879640	0.0675737378399486	0.0582067125108132
18	0.544949260913066	0.311399577664609	0.0882964747628847
19	0.577350269189626	0.577350269189626	0.104453135830172
20	0.544949260913066	0.778498944161523	0.0882964747628847
21	0.473016164879640	0.878458591919332	0.0582067125108141
22	0.581914373962646	0.145478593490662	0.0723426374612526
23	0.646761666763555	0.404226041727222	0.0985614419300660
24	0.646761666763555	0.646761666763555	0.0985614419300660
25	0.581914373962646	0.800132264198639	0.0723426374612526

Table B.1: T_7 Quadrature Set (continued).

i	ξ_i	η_i	W_i
26	0.242091013067521	0.060522753266880	0.0419359596096092
27	0.282138246343439	0.282138246343439	0.0660565456086300
28	0.311399577664609	0.544949260913066	0.0882964747628847
29	0.311399577664609	0.778498944161523	0.0882964747628847
30	0.282138246343439	0.916949300616178	0.0660565456086317
31	0.242091013067521	0.968364052270084	0.0419359596096101
32	0.333333333333333	0.133333333333333	0.0559374747989008
33	0.382359556450936	0.382359556450936	0.0838150329949681
34	0.404226041727222	0.646761666763555	0.0985614419300669
35	0.382359556450936	0.841191024192060	0.0838150329949681
36	0.333333333333333	0.933333333333333	0.0559374747989008
37	0.0524863881081478	0.052486388108147	0.0273981172069195
38	0.0605227532668803	0.242091013067521	0.0419359596096083
39	0.0675737378399486	0.473016164879640	0.0582067125108114
40	0.0705345615858599	0.705345615858598	0.0660962551843163
41	0.0675737378399486	0.878458591919332	0.0582067125108114
42	0.0605227532668803	0.968364052270084	0.0419359596096109
43	0.0524863881081478	0.997241374054808	0.0273981172069204
44	0.116051770637132	0.116051770637132	0.0370139280413842
45	0.133333333333333	0.333333333333333	0.0559374747989017
46	0.145478593490662	0.581914373962646	0.0723426374612544
47	0.145478593490662	0.800132264198639	0.0723426374612535
48	0.133333333333333	0.933333333333333	0.0559374747989008
49	0.116051770637132	0.986440050415621	0.0370139280413877

APPENDIX C: Code: Current Model

C.1. Main Code

```
command = 'fluent 2d -aas';
status = dos(command);
pause(15)
fluent = actxserver('ANSYS.CoFluentUnit.1');
tui=fluent.getSchemeControllerInstance();
fid=fopen('aaS_FluentId.txt','r');
fluentkey=fscanf(fid,'%s');
fclose(fid);
fluent.ConnectToServer (fluentkey);
tui.DoMenuCommand('file rc fff-6');
tui.DoMenuCommand('define user-defined interpreted-functions ...
    before.c () () ()');
ANN=tui.DoMenuCommandToString('it 500');
tui.DoMenuCommand('file export ascii thc.txt () no molef-co2 ...
    molef-h2o temperature () yes');
while length(ANN)>500
    mainWR
    fluent = actxserver('ANSYS.CoFluentUnit.1');
    tui=fluent.getSchemeControllerInstance();
    fid=fopen('aaS_FluentId.txt','r');
    fluentkey=fscanf(fid,'%s');
    fclose(fid);
    fluent.ConnectToServer (fluentkey);
    ANN=tui.DoMenuCommandToString('it 500');
    tui.DoMenuCommand('file export ascii thc.txt () no molef-co2 ...
        molef-h2o temperature () yes ok');
end
```

C.2. Radiation Solver: MainWR

```
Ts=300;
Tw=300;
Te=300;
Tn=300; %WALL TEMPERATURES
N=20;  %#of meshes in y direction
M=20;  %#of meshes in x direction
x_L=0.01; %x_L: geometry in x direction [m]
y_L=0.005; %y_L: geometry in y direction [m] %change  ...
    twodRTEsolver.m ALSO
x=x_L/(2*M):x_L/M:x_L-x_L/(2*M);  % x discretization
y=y_L/(2*N):y_L/N:y_L-y_L/(2*N);  % y discretization
areaEW=y_L/N;areaNS=x_L/M;  %area on Eeat West faces...
 %READING T CO2 and H2O values from file named thc.txt.
fid = fopen('thc.txt');
C = textscan(fid, ' %f','headerlines',1);
fclose(fid);
C=reshape(cell2mat(C),6,N*M);  %reshaping cell to matrix
T=reshape(transpose(C(4,:)),N,M);  %assign T values in matrix T (NxM)
CO2=reshape(transpose(C(6,:)),N,M);  %assign CO2 values in matrix  ...
    CO2 (NxM)
H2O=reshape(transpose(C(5,:)),N,M);  %assign H2O values in matrix  ...
    H2O (NxM)
 %PM260 returns k(g) values from lookup tables (dataco2 and  ...
    datah2o) for given T,CO2 and H2O accordingly
 %kappa_fieldco2(NxM cell) is k(g) of CO2 depending wavelength,  ...
    quadrature scheme and spatial coordinates TOTAL 20x20x96x7
 %kappa_fieldh2o(NxM cell) is k(g) of H2O depending wavelength,  ...
    quadrature scheme and spatial coordinates TOTAL 20x20x367x7
[kappa_fieldco2,kappa_fieldh2o, g ,wg,cont]=PM260(T,CO,H2O);
 %BBR7 returns blackbody emissions depending wavelength, T and  ...
    spatial coordinate
 %source_field(NxM cell) TOTAL 20x20x367
source_field=BBR7(T);
load logi;
checkco2=1:367;
```

```
checkh2o=checkco2(not(logi));
checkco2=checkco2(logi);
count=0;
sumdivq=zeros(N,M);
for I=1:96
    wn=checkco2(I);
    kappah2o=zeros();
    kappaco2=zeros();
    source_frac=zeros();
     %kappa ASSIGN wrt wavelength
    for i=1:N
        for j=1:M
            source_frac(i,j)=source_field{i,j}(1,wn);
            for G=1:7
                kappah2o(i,j,G)=kappa_fieldh2o{i,j}(wn,G);
                kappaco2(i,j,G)=kappa_fieldco2{i,j}(I,G);
            end
        end
    end
     %END ASSIGN
     %BEGIN CALCULATION FOR OVERLAPPED BANDS
    for G1=1:7
        for G2=1:7
            kappa=squeeze(kappaco2(:,:,G1))+squeeze(kappah2o(:,:,G2));
            source_frac2=source_frac.*kappa*areaEW*areaNS;
            divq=twodRTEsolver(kappa,source_frac2,wn);
            sumdivq=sumdivq+wg(G1)*wg(G2)*divq;
        end
    end
     %END CALCULATION
end
for I=1:367-96
    wn=checkh2o(I);
    for G=1:7
        kappah2o=zeros();
        source_frac=zeros();
        for i=1:N
            for j=1:M
```

```
67                  kappah2o(i,j)=kappa_fieldh2o{i,j}(wn,G);
68                  source_frac(i,j)=source_field{i,j}(1,wn);
69              end
70          end
71          source_frac=source_frac.*kappah2o*areaEW*areaNS;
72          divq=twodRTEsolver(kappah2o,source_frac,wn);
73          sumdivq=sumdivq+wg(G)*divq;
74      end
75  end
76   % % WRITING SOLUTION
77  fid = fopen('dohf.txt', 'wt');  % Open for writing
78  fprintf (fid, 'X [m]  Y [m] Div Heat Flux [W/m3]   n');
79  for j=1:size(T,2)
80      for i=1:size(T,1)
81         I=i;
82         fprintf (fid, ' %1.6f  %1.6f  %4.2f   n',x(j), y(I),  ...
               sumdivq(I,j));
83      end
84  end
85  fclose(fid);
```

C.3. User Defined Functions, cfd software

```
#include "udf.h"
#include "mem.h"
int eqn=6;
real dummy, dummy2, divq, source;
DEFINE_ADJUST(matlab_to_fluent)
{
    Domain *domain;
    cell_t c;
    Thread *t;
    int j;
    FILE *fp;
    domain=Get_Domain(1);
    fp = fopen("dohf.txt", "r");
    for (j=0; j<9; j++)
    {
        fscanf (fp, " %s",  &dummy3);
    }
    thread_loop_c (t, domain)
    {
        begin_c_loop (c, t)
        {
            fscanf(fp, " %f %f %f",  &dummy,  &dummy2,  &divq);
            C_UDMI(c, t, 0) = divq;
        }
        end_c_loop (c, t)
    }
    fclose(fp);
}
DEFINE_SOURCE(energy, c, t, dS, eqn)
{
    real source;
    source=C_UDMI(c, t, 0);
    dS[eqn] = 0;
    return source;
}
```

C.4. FLUENT UDF HOOKING

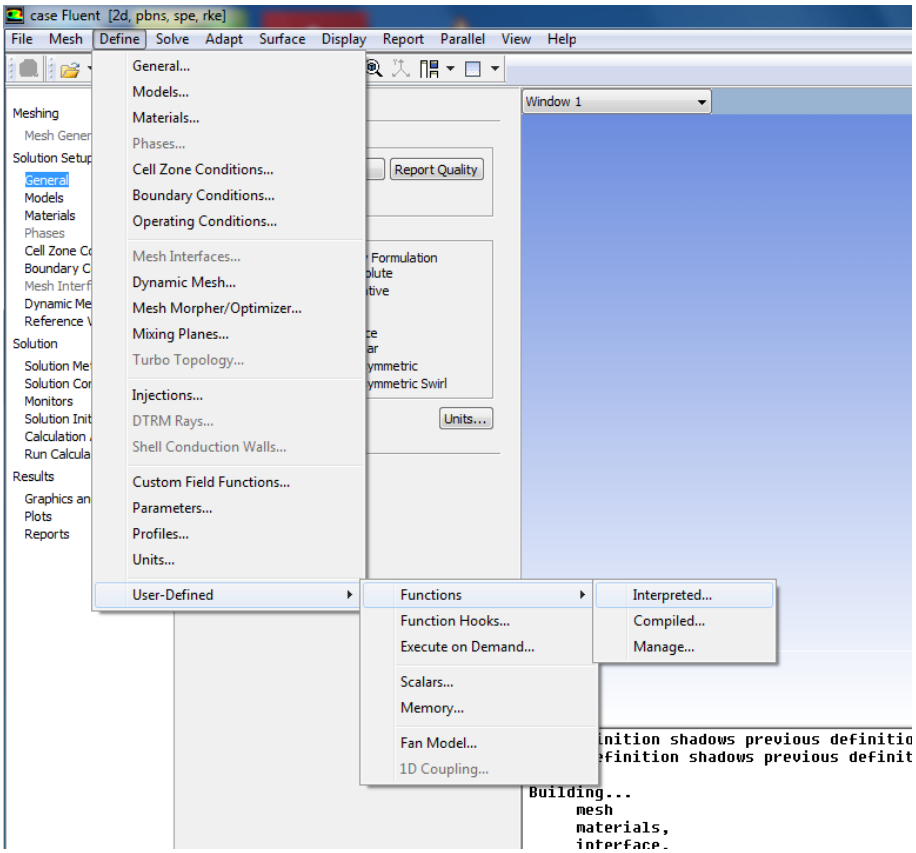

Figure C.1: Interpreting UDF.

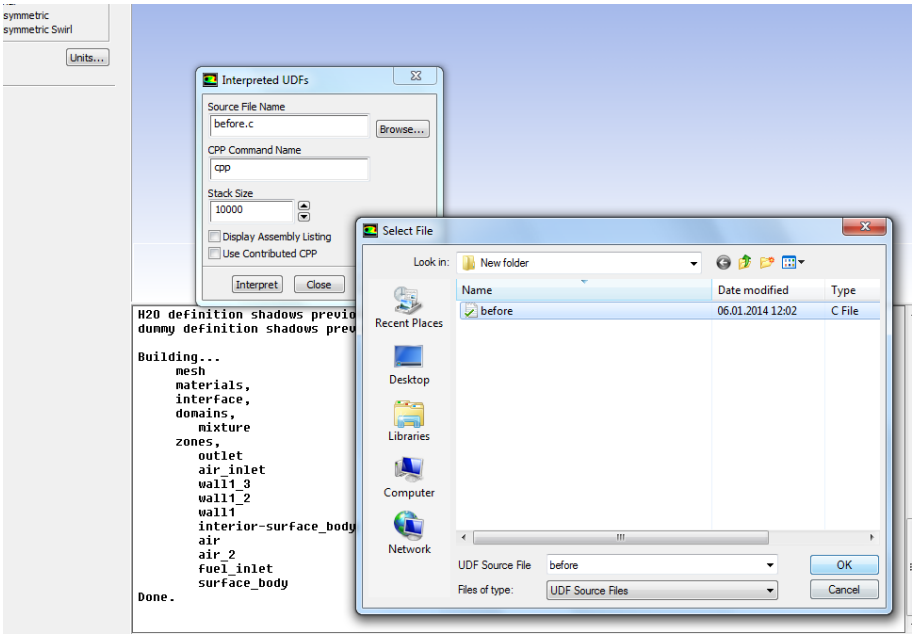

Figure C.2: Interpreting UDF 2.

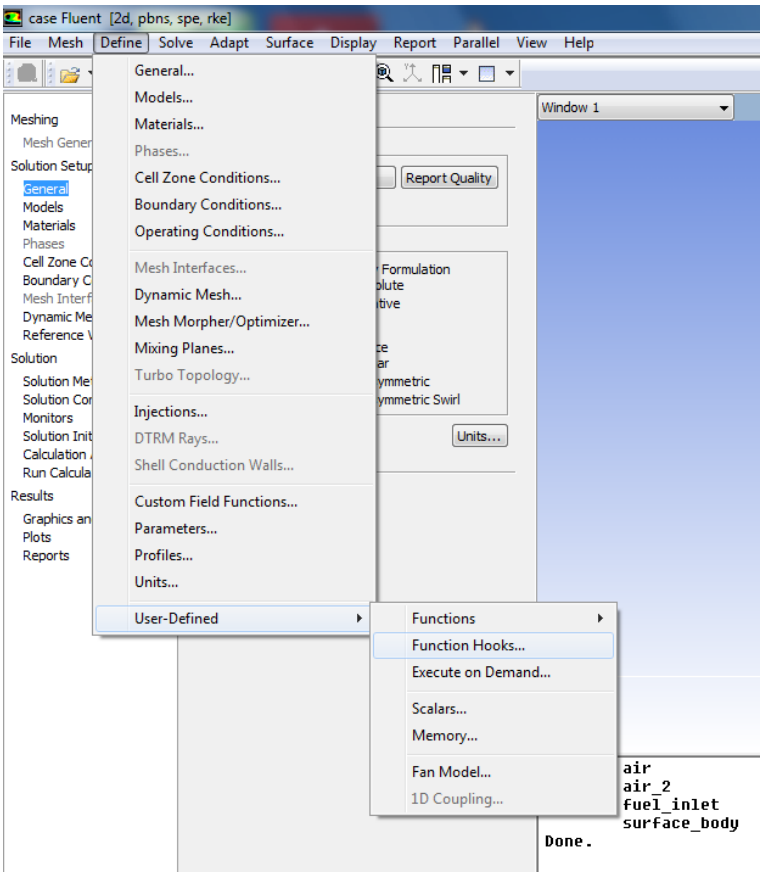

Figure C.3: Interpreting UDF 3.

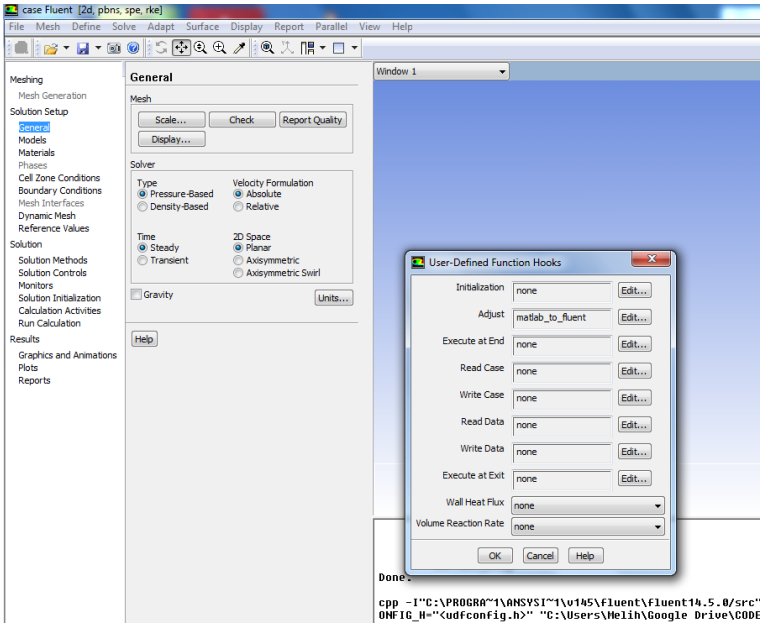

Figure C.4: Interpreting UDF 4.

REFERENCES

1. Modest, M. F., *Radiative Heat Transfer*, 3rd edition, Academic Press, Oxford, 2013.

2. Rothman L. S., I. E. Gordon, R. J. Barber, H. Dothe, R. R. Gamache, A. Goldman, V. I. Perevalov, S. A. Tashkun, J. Tennyson, "HITEMP, The High-Temperature Molecular Spectroscopic Database", *Journal of Quantitative Spectroscopy and Radiative Transfer*, Vol. 111, No. 15, pp. 2139-2150, 2010.

3. Rothman L. S., I. E. Gordon, A. Barbe, D. C. Benner, P. F. Bernath, M. Birk, V. Boudon, L. R. Brown, A. Campargue, J. P. Champion, K. Chance, L. H. Coudert, V. Danaj, V. M. Devi, S. Fally, J. M. Flaud, R. R. Gamache, A. Goldmanm, D. Jacquemart, I. Kleiner, N. Lacome, W. J. Lafferty, J. Y. Mandin, S. T. Massie, S. N. Mikhailenko, C. E. Miller, N. Moazzen-Ahmadi, O. V. Naumenko, A. V. Nikitin, J. Orphal, V. I. Perevalov, A. Perrin, A. Predoi-Cross, C. P. Rinsland, M. Rotger, M. Simeckova, M. A. H. Smith, K. Sung, S. A. Tashkun, J. Tennyson, R. A. Toth, A. C. Vandaele, J. VanderAuwera, " The HITRAN 2008 Molecular Spectroscopic Database", *Journal of Quantitative Spectroscopy and Radiative Transfer*, Vol. 110, No. 9, pp. 533-572, 2009.

4. Lacis, A., V. Oinas, "A Description of the Correlated-k Distribution Method for Modeling Non-gray Gaseous Absorption, Thermal Emission and Multiple Scattering in Vertically Inhomogeneous Atmospheres", *Journal of Geophysical Research: Atmospheres*, Vol. 96, No. D5, pp. 9027-9063, 1991.

5. Modest, M. F., "Narrow-Band and Full-Spectrum K-Distributions for Radiative Heat Transfer – Correlated-k vs. Scaling Approximation", *Journal of Quantitative Spectroscopy and Radiative Transfer*, Vol. 76, No. 1, pp. 69-83, 2003.

6. Goutire, V., A. Charette, L. Kiss, "Comparative Performance of Nongray Gas Modeling Techniques", *Numerical Heat Transfer, Part B*, Vol. 41, No. 5, pp. 361-381, 2002.

7. ANSYS, Inc., "Ansys Fluent", 2014, http://www.ansys.com/Products/Simulation+Technology/Fluid+Dynamics/Fluid+Dynamics+Products/ANSYS+Fluent, [Accessed July 2014].

8. The MathWorks, Inc., "MATLAB: The Language of Technical Computing", 2014, http://www.mathworks.com/products/matlab/, [Accessed July 2014].

9. Goutiere V., F. Liu, A. Charette, "An Assessment of Real-gas Modeling in 2D Enclosures", *Journal of Quantitative Spectroscopy and Radiative Transfer*, Vol. 64, No. 3, pp. 299-326, 2000.

10. Howell, J. R., R. Siegel, M. P. Mengüç, "Thermal Radiation Heat Transfer", 5th edition, Taylor and Francis, New York, 2011.

11. Carvalho, M. G., T. L. Farias, "Modeling of Heat Transfer in Radiating and Combusting Systems", *Transactions of Institution of Chemical Engineers*, Vol. 76, pp. 175-184, 1998.

12. Viskanta, R., "Computation of Radiative Transfer in Combustion Systems", *International Journal of Numerical Methods for Heat and Fluid Flow*, Vol. 18, No. 3, pp. 415-442, 2008.

13. Hottel, H. C., "Radiant Heat Transmission", 3rd edition, W. H. McAdam, McGraw-Hill, New York, 1954.

14. Bergman, T. L., A. S. Lavine, F. P. Incropera, D. P. DeWitt, 'Fundamentals of Heat and Mass Transfer", 7th edition, John Wiley and Sons, Hoboken, NJ, 2011.

15. Leckner, B., "Spectral and Total Emissivity of Water Vapor and Carbon Dioxide", *Combustion and Flame*, Vol. 19, No. 1, pp. 33-48, 1972.

16. Wang, P., F. Fan, Q. Li, "Accuracy Evaluation of the Gray Gas Radiation Model in CFD simulation", *Case Studies in Thermal Engineering*, Vol. 3, pp. 51-58, 2014.

17. Hottel, H. C., A. F. Sarofim, "Radiative Transfer", McGraw-Hill, New York, 1967.

18. Mazumder, S., M. F. Modest, "Application of the Full Spectrum Correlated-k Distribution Approach to Modeling Non-Gray Radiation in Combustion Gases", *Combustion and Flame*, Vol. 129, No. 4, pp. 416-438, 2002.

19. Elsasser, W. M., "Heat Transfer by Infrared Radiation in the Atmosphere", Harvard University Press, Cambridge, MA, 1943.

20. Malkmus, W., "Random Lorentz Band Model with Exponential-Tailed S1 Line-Intensity Distribution Function", *The Journal of the Optical Society of America*, Vol. 57, No. 3, pp. 323-329, 1967.

21. Smith, T. F., Z. F. Shen, J. N. Friedman, "Evaluation of Coefficients for the Weighted Sum of Gray Gases Model", *ASME Journal of Heat Transfer*, Vol. 104, No. 4, pp. 602-608, 1982.

22. Farag, I. H., T. A. Allam, "Gray-gas Approximation of Carbon Dioxide Standard Emissivity", *ASME Journal of Heat Transfer*, Vol. 103, No. 2, pp. 403-405, 1981.

23. Taylor, P. B., P. J. Foster, "Some Gray Gas Weighting Coefficients for CO_2H_2OSoot Mixtures", *International Journal of Heat and Mass Transfer*, Vol. 18, No. 11, pp. 1331-1332, 1975.

24. Goody, R. M., Y. L. Yung, "Atmospheric Radiation", 2nd edition, Oxford University Press, Oxford, 1989.

25. Liu, F., G. J. Smallwood, Ö. L. Gülder, "Application of the Statistical Narrow-band Correlated-k Method to Low-resolution Spectral Intensity and Radiative Heat Transfer Calculations Effects of the Quadrature Scheme", *International Journal of Heat and Mass Transfer*, Vol. 43, No. 17, pp. 2227-2236, 2000.

26. Ludwig, D. B., W. Malkmus, J. E. Reardon, J. A. L. Thomson, "Handbook of Infrared Radiation from Combustion Gases", *NASA SP3080*, Washington D.C.,

1973.

27. Soufiani, A., J. Taine, "High Temperature Gas Radiative Property Parameters of Statistical Narrow-band Model for H_2, CO_2 and CO and Correlated-K Model for H_2O and CO_2", *International Journal of Heat and Mass Transfer*, Vol. 40, No. 4, pp. 987-991, 1997.

28. Domoto, G. A., "Frequency integration for Radiative Transfer Problems Involving Homogeneous Non-gray Gases: The Inverse Transmission Function", *Journal of Quantitative Spectroscopy and Radiative Transfer*, Vol. 14, No. 9, pp. 935-942, 1974.

29. Chu, H., F. Liu, H. Zhou, "Calculations of Gas Radiation Heat Transfer in a Two-dimensional Rectangular Enclosure Using the Line-by-line Approach and the Statistical Narrow-band Correlated-k Model", *International Journal of Thermal Sciences*, Vol. 59, pp. 66-74, 2012.

30. Thurgood, C. P., A. Pollard, H. A. Becker, "The Tn Quadrature Set for the Discrete Ordinates Method", *Transactions of the ASME*, Vol. 117, No. 4, pp. 1068-1070, 1995.

31. Coppalle, A., P. Vervisch, "The Total Emissivities of High Temperature Flames", *Combustion and Flame*, Vol. 49, No. 1, pp. 101-108, 1983.

32. Denison, M. K., B. W. Webb "A Spectral Line-Based Weighted-Sum-of-Gray-Gases Model for Arbitrary RTE Solvers", *Journal of Heat Transfer*, Vol. 115, No. 4, pp. 1004-1012, 1993.